

## Detailed Kinetics and Thermochemistry of $C_2H_5 + O_2$ : Reaction Kinetics of the Chemically-Activated and Stabilized $CH_3CH_2OO\cdot$ Adduct

Chad Y. Sheng<sup>†</sup> and Joseph W. Bozzelli\*

Departments of Chemical Engineering, Chemistry and Environmental Science,  
New Jersey Institute of Technology, Newark, New Jersey 07102

Anthony M. Dean

Chemical Engineering Department, Colorado School of Mines, Golden, Colorado 80401

Albert Y. Chang

Jet Propulsion Laboratory, California Institute of Technology, Pasadena, California 91109

Received: December 17, 2001; In Final Form: April 9, 2002

The kinetics of the chemically activated reaction between the ethyl radical and molecular oxygen are analyzed using quantum Rice–Ramsperger–Kassel (QRRK) theory for  $k(E)$  with both a master equation analysis and a modified strong-collision approach to account for collisional deactivation. Thermodynamic properties of species and transition states are determined by ab initio methods at the G2 and CBS-Q//B3LYP/6-31G(d,p) levels of theory and isodesmic reaction analysis. Rate coefficients for reactions of the energized adducts are obtained from canonical transition state theory. The reaction of  $C_2H_5$  with  $O_2$  forms an energized peroxy adduct with a calculated well depth of 35.3 kcal mol<sup>-1</sup> at the CBS-Q//B3LYP/6-31G(d,p) level of theory. The calculated (VTST) high-pressure limit bimolecular addition reaction rate constant for  $C_2H_5 + O_2$  is  $2.94 \times 10^{13} T^{-0.44}$ . Predictions of the chemically activated branching ratios using both collisional deactivation models are similar. All of the product formation pathways of ethyl radical with  $O_2$ , except the direct  $HO_2$  elimination from the  $CH_3CH_2OO\cdot$  adduct, involve barriers that are above the energy of the reactants. As a result, formation of the stabilized  $CH_3CH_2OO\cdot$  adduct is important at low to moderate temperatures; subsequent reactions of this adduct should be included in kinetic mechanisms. The temperature and pressure dependent rate coefficients for both the chemically activated reactions of the energized adducts and the thermally activated reactions of the stabilized adducts are assembled into a reaction mechanism. Comparisons of predictions using this mechanism to experiment demonstrate the necessity of including dissociation of the stabilized ethylperoxy adduct. Two channels are particularly important, direct  $HO_2$  elimination and reverse reaction to  $C_2H_5 + O_2$ , where the ratio of these rates is a function of temperature and pressure. The predictions, using unadjusted rate coefficients, are consistent with literature observations over extended temperature and pressure ranges. Comparison of a mechanism using  $7 \times 3$  Chebyshev polynomials to represent  $k(T,P)$  to a conventional mechanism which used  $k(T)$  only (different values for  $k(T)$  at different pressures) showed good agreement. The kinetic implications for low-temperature ignition due to the direct formation of ethylene and  $HO_2$  from ethylperoxy are discussed.

### Introduction

Reactions of hydrocarbon radicals with molecular oxygen are important in atmospheric chemistry as well as in combustion processes. The intermediates include energized and stabilized peroxy radicals, both of which can react back to reactants, isomerize, or react to new products. The initially formed energized peroxy radical has multiple reaction possibilities. The  $C_2H_5 + O_2$  reaction represents an important model system to explore the kinetic consequences of these reactions; it contains many of the complexities of larger systems yet is more amenable to higher level electronic structure calculations. An added advantage is that this reaction has been well studied experimentally.<sup>1–8</sup> These experiments will be detailed in the modeling and comparison section.

There have also been several theoretical analyses of this system.<sup>1,9–16</sup> Wagner et al.<sup>13</sup> have analyzed the  $C_2H_5 + O_2$  reaction using variational RRKM theory for ethylene production and ethyl radical loss at pressures and temperatures relevant to the experimental data of Slagle et al.<sup>3,7</sup> Their analysis assumes formation of a chemically activated adduct, which can react directly through a cyclic (five-member ring) intermediate to a primary hydroperoxyalkyl radical and then to  $C_2H_4 + HO_2$  or be stabilized to  $CH_3CH_2OO\cdot$ . Subsequent reaction of the stabilized peroxy back to reactants or forward, over the isomerization barrier, to ethylene +  $HO_2$  is accounted for with an analytical solution to a four-reaction mechanism, which assumes the kinetics depend only on the reactions leading to and including formation of the cyclic intermediate (excludes stabilization of the alkylhydroperoxy intermediate). The height of this barrier was adjusted to model the experimental data.

<sup>†</sup> Current address: Chemical Engineering Department, Colorado School of Mines, Golden, CO 80401.

Recent high-level *ab initio* calculations<sup>17</sup> have characterized a new concerted elimination path to directly produce C<sub>2</sub>H<sub>4</sub> and HO<sub>2</sub> from the initially formed ethylperoxy adduct. This pathway was not considered in earlier kinetic analyses of the ethyl + O<sub>2</sub> system<sup>9,13</sup> but was included in a recent study.<sup>18</sup> One important aspect of this system is that most of the reaction channels of the energized adduct are higher in energy than the entrance channel, but this new concerted elimination channel is a few kcal mol<sup>-1</sup> lower. This suggests that adduct stabilization is likely over an extended temperature range. Both Kaiser and Clifford *et al.* recognized the need to consider the kinetic consequences of subsequent thermal dissociation of this adduct in analyzing their experimental data.<sup>1,2</sup> The dissociation reactions become increasingly important at higher temperatures, where the rate coefficients are larger.

We use electronic structure theory to generate all the input parameters needed to analyze this chemically activated system. We assess whether this approach can accurately predict the temperature and pressure dependence of the various reaction channels. The potential energy surface is calculated at relatively high levels, and the rate coefficients for reactions of the energized adducts are obtained from canonical transition state theory (CTST). The rate coefficient for initial formation of ethylperoxy is calculated using variational transition state theory (VTST). We compare two models for collisional deactivation in conjunction with use of a multi-frequency QRRK analysis to estimate  $k(E)$ . Finally, we incorporate the predictions for the individual branching fractions of the energized adducts and those for thermal dissociation of the stabilized adducts into a mechanism to illustrate where it is necessary to account for thermal dissociation. Comparison of model with experiment suggests that this approach, with no adjustments to any of the parameters, permits an accurate description of this system. The results for loss of ethyl and production of ethylene show good agreement with recent experimental data of Kaiser.<sup>1</sup> Good agreement was also obtained for HO<sub>2</sub> production measurements of Clifford *et al.*<sup>2</sup> We also explore the kinetic implications of the direct formation of ethylene and HO<sub>2</sub> from CH<sub>3</sub>CH<sub>2</sub>OO\*.

The rate coefficients calculated by the QRRK/master equation analysis vary with both temperature and pressure. A conventional CHEMKIN mechanism would therefore need different sets of rate coefficients  $k(T)$  for each pressure. Instead of many mechanisms for evaluation vs pressure, we use Chebyshev polynomial fits<sup>19,20</sup> to capture  $k(T,P)$  in one rate expression. The result is one set of rate coefficients (one mechanism) that applies to all pressures. We introduce a modification to the CHEMKIN integrator package<sup>21</sup> to accept rate constants in the form of a Chebyshev expression. This allows use of a single mechanism to cover a wide range of temperatures and pressures.

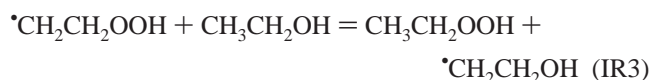
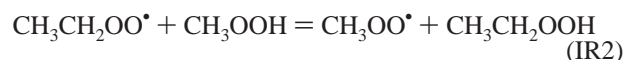
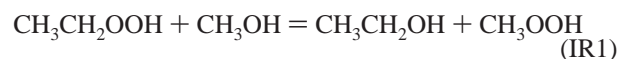
## Computational Methods

### Ab Initio and Density Functional Theory Computations.

Molecular properties for reactants, adducts, transition states (TS), and products are estimated by high level CBS-Q<sup>22</sup> *ab initio* calculations and by density functional theory (DFT). The *ab initio* and DFT calculations are performed using Gaussian94.<sup>23</sup> The hybrid DFT method B3LYP, which combines the three parameter Becke exchange functional, B3, with the Lee–Yang–Parr nonlocal correlation functional, LYP, with a double- $\zeta$  polarized basis set, 6-31G(d,p), is used to determine the optimized geometry.<sup>24,25</sup> Single point calculations at the complete basis set, composite method-CBS-Q are utilized on the basis of the optimized B3LYP/6-31G(d,p) geometry, denoted as CBS-Q//B3LYP/6-31G(d,p). The DFT calculations are spin-

unrestricted Hartree–Fock. Molecular geometries at B3LYP/6-31G(d,p) are fully optimized using the Berny algorithm and redundant internal coordinates.<sup>23</sup> The geometries of the five TS structures in this system are verified by checking for one imaginary frequency and consistency in bond lengths characteristic of a TS. Comparison of geometric structures are also performed with those determined by Rienstra-Kiracofe *et al.*'s high-level coupled cluster methods.<sup>17</sup> Zero-point vibrational energy (ZPVE), vibrational frequencies, and thermal correction contributions to enthalpy from harmonic frequencies are scaled in accordance to the scaling factors recommended by Scott and Radom.<sup>26</sup> The inclusion of ZPVE and thermal corrections to the total energies of the species in this system has been applied accordingly.

Enthalpies of the two adducts are determined by use of isodesmic working reactions with group balance. Fundamental requirements for an isodesmic reaction are conservation of electron pair and chemical bond type.<sup>27</sup> The use of isodesmic reactions is an accurate and desired method for estimating enthalpy of formation. Three isodesmic reactions are employed to determine the enthalpy of formation for the two adducts of interest, *viz.*



The enthalpies of formation for the adducts of interest are the ethylperoxy radical in (IR2) and the hydroperoxyethyl radical in (IR3). The enthalpies of formation for all the other oxyhydrocarbon species in the respective isodesmic reactions are needed before we can determine the enthalpy of formation of the two desired adducts. (IR1) is utilized to determine the enthalpy of formation for the ethyl–hydroperoxide molecule, which is then used in (IR2) and (IR3) to aid in the determination of the ethylperoxy radical and hydroperoxyethyl radical. It is important to note that the enthalpies of the ethylperoxy and hydroperoxyethyl radicals are determined independently and on an absolute scale. The difference in these two enthalpy values is our  $\Delta H_{\text{rxn}}$  between the two isomers (adducts).

The barrier for isomerization is determined from the average difference between the energy calculated for the TS and the energies of both reactant  $E_c(\text{CH}_3\text{CH}_2\text{OO}^*)$  and product  $E_c(^*\text{CH}_2\text{CH}_2\text{OOH})$ , with ZPVE and thermal corrections included. Enthalpy of formation of the two adducts (reactant and product) and  $\Delta H_{\text{RXN}}$  are from the isodesmic reaction analysis. The average activation energy barrier for the TS is now determined relative to enthalpy of the two isomers.

$$\Delta H_{\text{RXN}} = \Delta_f H_{298} (^*\text{CH}_2\text{CH}_2\text{OOH}) - \Delta_f H_{298} (\text{CH}_3\text{CH}_2\text{OO}^*)$$

from isodesmic reaction analysis

$$\Delta H_{\text{TS-R}} = E_c(\text{TS}) - E_c(\text{CH}_3\text{CH}_2\text{OO}^*)$$

$$\Delta H_{\text{TS-P}} = [E_c(\text{TS}) - E_c(^*\text{CH}_2\text{CH}_2\text{OOH})] + \Delta H_{\text{RXN}}$$

$$\Delta H_{\text{barrier}} = \frac{\Delta H_{\text{TS-P}} + \Delta H_{\text{TS-R}}}{2}$$

A comparative study of G2<sup>28</sup> vs CBS-Q on the two adducts in

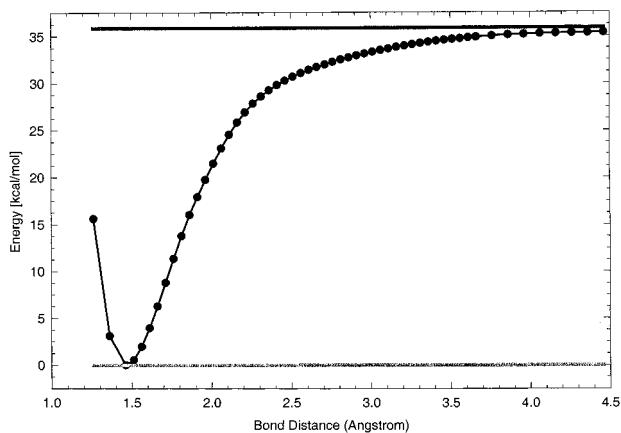


**Figure 1.** Reaction coordinate of the dissociation reaction of  $\text{CH}_3\text{-CH}_2\text{OO}^* \rightarrow \text{C}_2\text{H}_5 + \text{O}_2$  as the C–O bond increases, calculated at B3LYP/6-31G(d,p).

the ethyl radical oxidation system is also performed. The “standard” G2 calculation, using the MP2(FU)/6-31G(d) method to optimize the geometry, is used. Comparison of the two high level, composite ab initio methods, G2 and CBS-Q/B3LYP/6-31G(d,p) implies good accuracy of the enthalpy of formation for the two adducts in this system.

A standard statistical mechanical analysis was employed to determine the vibrational, external rotational, and translational contributions to entropy and  $C_p(T)$ . Molecular parameters required in the statistical mechanic analysis are calculated at the B3LYP/6-31G(d,p) level of theory for the optimized geometric structure of the species. Vibrational contributions to entropy and  $C_p$  are scaled by the recommended scaling factors from Scott and Radom.<sup>26</sup> Optical isomers and unpaired electrons are also included in the  $S_{298}$  and  $C_p(T)$  calculations accordingly. Contributions of internal rotation to  $S_{298}$  and  $C_p(T)$  are incorporated based on the Pitzer-Gwinn formalism.<sup>29</sup>

**Calculation of High-Pressure Rate Constants.** The high-pressure forward rate constants for most reactions were determined by application of CTST for temperatures from 300 to 2500 K. Forward rate constants from 300 to 2500 K are calculated and fitted by a nonlinear least-squares method to the form of a modified Arrhenius rate expression, i.e.

$$k_{\infty, \text{forw}} = A_{\infty} T^n e^{-E_a/RT}$$

The rate constants for the addition and dissociation reaction for  $\text{C}_2\text{H}_5 + \text{O}_2 \leftrightarrow \text{CH}_3\text{CH}_2\text{OO}^*$  are calculated by VTST at the B3LYP/6-31G(d,p) level. The reaction coordinate along the C–O bond length is calculated to determine the total energy (Figure 1). Rate constants are calculated on the basis of the most favorable dissociation pathway along the reaction surface. The addition reaction rate constant is determined by satisfying the detailed balance criteria.

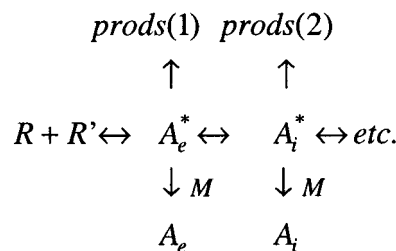
**Kinetic Analysis: Modified Strong Collision and Master Equation.** Two approaches are used to calculate the collisional deactivation of the energized adduct: a master equation model and a modified strong collision model. The master equation model (ME) used  $\langle \Delta E \rangle_{\text{down}} = 830 \text{ cal mol}^{-1}$  for the collisional deactivation with  $\text{N}_2$  as the third body. The modified strong collision model (MSC) of Gilbert et al.<sup>30</sup> was used with  $\langle -\Delta E \rangle_{\text{av}} = 440 \text{ cal mol}^{-1}$  for the collisional deactivation with  $\text{N}_2$  as the third body. This value is consistent with the  $\langle \Delta E \rangle_{\text{down}}$  value used in the master equation analysis.

**Calculation of  $k(T, P)$ .** Kinetic parameters for the bimolecular chemical activation reactions and the subsequent unimolecular

thermal dissociation reactions to adducts and product sets are calculated by using a multifrequency quantum Rice–Ramsperger–Kassel (QRRK) analysis for  $k(E)$ <sup>31</sup> with the steady-state assumption on the energized adduct(s). Both the forward and reverse paths are included for adducts, but product formation is not reversible in the analysis. (Reverse directions of products are incorporated in the subsequent mechanism analysis using CHEMKIN.)

The current version of the QRRK computer code utilizes a reduced set of three vibration frequencies that accurately reproduce the molecule (adduct) heat capacity data.<sup>32–34</sup> Molecular density-of-state functions are constructed through direct convolution of single frequency density functions on a  $10 \text{ cm}^{-1}$  grid. The functions corresponding to each reduced frequency are explicitly convolved into a relative density-of-states ( $\rho(E)$ ), which is normalized by the partition function ( $Q$ ). The inclusion of one external rotation, corresponding to the symmetric top, is incorporated into the calculations by convolving the vibration density function with the proper rotational density function. A detailed description of this and comparisons of the  $\rho(E)/Q$  ratios with the direct count  $\rho(E)/Q$  ratios are shown to be in good agreement.<sup>34</sup>

**Master Equation Model for Chemical Activation.** Our primary interest is in solving chemically activated bimolecular reactions of the type



where  $A_i^*$  denotes an activated complex,  $A_i$  its stabilized adduct, and prods(p) denotes one of several product channels. The subscript  $e$  identifies that isomer formed directly by the initial reactants  $R$  and  $R'$ . Subsequent isomerizations can lead to other complexes that can dissociate to form various products, re-isomerize, or collisionally de-energize to form stabilized adducts. The entrance isomer can also dissociate back to reactants, and this can effectively be treated as another product channel. The overall bimolecular rate constants from reactants to either stabilized adducts or products are defined via

$$\frac{d[A_i]}{dt} = [R][R']k_i^{\text{stab}}(T, P) \quad (\text{MEM1})$$

$$\frac{d[\text{prods(p)}]}{dt} = [R][R']k_p^{\text{prod}}(T, P) \quad (\text{MEM2})$$

The goal is to calculate the rate constants  $k_i^{\text{stab}}$  and  $k_p^{\text{prod}}$  as functions of temperature, pressure, and the collision parameters of the surrounding molecules.

The master equation can be written by applying the steady-state condition to balance the flux into and out of each level,

$$f_i^q + \sum_j k_{ij}^q n_j^q + \omega \sum_r P_i^{qr} n_i^r = n_i^q (\sum_p d_{p,i}^q + \sum_j k_{ji}^q + \omega) \quad (\text{MEM3})$$

Here, isomers are denoted by subscripts  $i$  and  $j$  ( $i, j = 1, n$ ) and energy levels are denoted by superscripts  $q$  and  $r$  ( $q, r = q_0^i, q_{\text{max}}$ ). Typically, the energy grid is defined on an interval

between 0.3 and 1.0 kcal. The index  $q_0^i$  corresponds to the lowest energy for isomer  $i$ , and  $q_{\max}$  corresponds to the highest energy level considered for the system as a whole. Each isomer is also characterized by an energy level  $q_{\min}^i$ . This is the lowest energy level of the isomer that is assumed to be activated; levels below this value are considered stabilized. A collision from a level above this stabilization threshold to one below removes that participant from the system.  $q_{\min}^i$  is set a few collisions below the lowest exit channel for each isomer.

The vector  $f_i^q$  represents the differential input rate constant into level  $(i, q)$  due to the reactant channel. The matrix  $k_{ij}^q$  specifies the isomerization rate from isomer  $j$  to isomer  $i$  at energy level  $q$  (all isomerizations occur at constant energy). The differential rate constant for dissociation from isomer  $i$  to product channel  $p$  at energy  $q$  is denoted by  $d_{p,i}^q$ . Collisions, which occur at frequency  $\omega$ , can redistribute the energy level populations within a given isomer. The probability matrix  $P_i^{qr}$  denotes the probability of a collision resulting in a change from level  $r$  to level  $q$  of isomer  $i$ . Every collision is assumed to result in some energy change, so that the sum of  $P_i^{qr}$  from  $q_0^i$  to  $q_{\max}$  is unity.

The system of eqs MEM3 is solved for the population vectors  $n_i^q$ , which are functions of temperature, pressure, and collider molecule properties. The overall rate constant for any product channel is obtained by summing the differential rate constant times the population,

$$k_p^{\text{prod}}(T, P) = \sum_q d_{p,i}^q n_i^q \quad (\text{MEM4})$$

The rate constant for formation of a stabilized adduct is found by summing the product of population, collision frequency, and the fraction of deactivating collisions,

$$k_i^{\text{stab}}(T, P) = \omega \sum_r \left(1 - \sum_{q > q_{\min}^r} P_i^{qr}\right) n_i^r \quad (\text{MEM5})$$

*Collision Model.* The frequency of collisions between the adduct molecule and bath gas species is described using the standard Lennard-Jones model,

$$\omega = [M] N_A \pi \sigma^2 \Omega^{[2,2]}(T) \sqrt{\frac{8kT}{\pi\mu}} \quad (\text{MEM6})$$

Here  $[M]$  is the concentration of colliders,  $N_A$  is Avogadro's number,  $\sigma$  is the collision diameter, and  $\mu$  is the reduced mass of the collision. The collision integral  $\Omega^{[2,2]}(T)$  is given by the fit<sup>35</sup>

$$\Omega^{[2,2]}(T) = a_1 (kT/\epsilon)^{-c_1} + a_2 \exp(-c_2 kT/\epsilon) + a_3 \exp(-c_3 kT/\epsilon) \quad (\text{MEM7})$$

where  $a_1 = 1.16145$ ,  $a_2 = 0.52487$ ,  $a_3 = 2.16178$ ,  $c_1 = 0.14874$ ,  $c_2 = 0.77320$ , and  $c_3 = 2.43787$  and  $\epsilon$  is the geometric mean  $[(\epsilon_1\epsilon_2)^{1/2}]$  of the Lennard-Jones parameters of complex and collider. If necessary, (MEM6) can be easily generalized for a mixture of colliders.

An exponential down model is used for the collision probability. This assumes the probability of energy transfer from a level  $r$  to a level  $q$  of lower energy is proportional to the exponential of the energy difference,

$$P_{\text{down}}^{qr} = \frac{1}{N_r} \exp(-(E_r - E_q)/\Delta E_{\text{down}}) \quad (\text{MEM8})$$

Here,  $N_r$  is a normalization constant which must be determined. The probability of energy transfer to a higher level is found by the detailed balance equation,

$$\rho_j(E_q) P_{\text{up}}^{rj} e^{-E_q/RT} = \rho_j(E_r) P_{\text{down}}^{qr} e^{-E_r/RT} \quad (\text{MEM9})$$

where  $\rho_i(E)$  denotes the density function of isomer  $i$ . The term  $\Delta E_{\text{down}}$  in (MEM8) must be specified as a function of temperature. Presently, this is assumed to be of the form

$$\Delta E_{\text{down}}(T) = \Delta E_{\text{down}}(300) \left(\frac{T}{300}\right)^N \quad (\text{MEM10})$$

The creation of the  $P_i^{qr}$  matrix for each isomer is computationally straightforward. (MEM8) is used to fill the upper half of the matrix, sans normalization. When this is completed, the last column (that corresponding to collisions originating from  $q_{\max}$ ) is completely filled. This column is then normalized, and (MEM9) is used to "transpose" the column to fill the corresponding row. These row values are exact and require no further normalization. This operation fills the second-to-last column, and the lower half of this column is used to determine the normalization constant of the upper half. The process is continued until the entire matrix is filled and normalized. Potential difficulties can arise in the first few columns (last to be filled) because the constraints independently imposed by (MEM8) and (MEM9) may conflict. For example, the sum of probabilities in the lower half of the column may exceed unity, and no correction to the top half of the column can correct this. This is not a serious difficulty since these first few levels are below the stabilization threshold and have a negligible effect on the overall rate constants. For mathematical consistency the offending columns are simply renormalized.

*Rates and Density of State Functions.* In this implementation, differential rate constants are constructed using the modified QRRK method as described in a separate paper.<sup>31</sup> These techniques enable the calculation of energy dependent rate constants based on the density function of each parent isomer and several coefficients describing the temperature dependence of dissociation in the high-pressure limit. These methods have the advantage over RRKM in that detailed transition state information is not required. The high-pressure limiting rate constants needed as input are calculated via CTST.

In (MEM3), provision is made for multiple input pathways to the system. This could describe the case where the same reactants could directly combine to form several different initial adducts. However, the system of equations is linear, and this makes solutions superimposable. It is thus sensible to treat each reactant pathway separately. This facilitates interpretation of the results at the minor expense of having to handle a few more rate constants. In this approach, all  $f_i^q$  are zero except those that correspond to the formation of initial isomer ( $i = e$ ),

$$f_i^q = k_{-s}^{\text{rxn}}(E) \delta_{ie} \quad (\text{MEM11})$$

Here  $k_{-s}^{\text{rxn}}(E)$  is the differential rate constant for the reactants to form entrance isomer  $e$ . The subscript  $-s$  denotes this is the reverse reaction to that which forms product channel  $s$ .

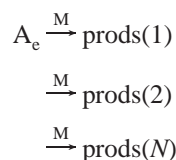
*Solution Algorithm.* The master equation analysis of chemical activation is significantly complicated when the activated adduct is allowed to undergo multiple isomerizations. This is because the master equation (MEM3) incorporates matrices indexed by both energy and isomer number. Fortunately, Carter and Tardy<sup>36</sup> showed how this problem can be conceptually treated as solving a succession of  $2 \times 2$  matrix equations. Although they used

their method in conjunction with RRKM theory, the analysis is the same whatever model  $k(E)$  is adopted. Carter and Tardy provide detailed derivations and illustrative examples of their solution to this multi-isomerization problem. In the Appendix we outline their prescription, providing an alternate nomenclature to supplement their discussion. We also present what we feel is a simpler algorithm for the implementation of this solution.

**Master Equation Model for Dissociation.** The chemical activation analysis allows one to calculate effective elementary rate constants to form both product channels and stabilized adducts from the specified reactants. Rate constants thus generated can be incorporated into a chemical kinetic model. In these models, the application of microscopic reversibility provides reverse reaction rate constants for these same reactions. However, in many cases additional rate constants must be specified to complete the system. For example, although microscopic reversibility will give an effective rate constant for a stabilized adduct to form the initial reactants, this is often not the favored channel for dissociation. Thus a dissociation analysis that complements the chemical activation treatment is desired.

Unfortunately, a time-independent master equation solution for dissociation that allows for multiple isomerization is not possible.<sup>37</sup> The chemical activation problem can be treated by a steady state analysis; the reactant channel provides a continuous input, while the product and stabilization channels provide steady outputs. The dissociation analysis starts with an adduct population; any dissociation depletes this population. This is an eigenvalue problem in which the eigenvector solution describes a population distribution that decays with time with an invariantly shaped profile (and the decay rate itself is the eigenvalue). This analysis cannot easily accommodate other isomers. Either the isomerization processes must be assumed irreversible (i.e., all isomers created are immediately stabilized), in which case they are treated just as other product channels, or all isomers are assumed to be in some kind of equilibrium, in which case their populations cannot be specified separately. Outlined here is the former case of unimolecular dissociation to multiple product channels and irreversible isomerizations. This provides reasonable dissociation pathways for all adducts and provides rate constants in a form easily incorporated in a kinetic model. In cases where multi-isomerization dissociation is especially important, this analysis may be inadequate and more complicated strategies may need to be devised.

The single-isomer dissociation problem can be represented thus,



where, again, isomerizations are treated as irreversible product channels. The pressure-dependent dissociation rate constants are defined through the relation

$$\frac{d[\text{prods}(p)]}{dt} = [A_i]k_p^{\text{prod}}(T,P) \quad (\text{MEM12})$$

The master equation solution of this problem is implemented following the description in Gilbert and Smith.<sup>37</sup> Since multi-isomerization is not considered, the solution for each dissociating isomer is independent and must be solved separately. However,

the notation here is kept as much as possible consistent with that presented above.

In the dissociation problem, no distinction is made between activated and stabilized adduct. Rather there is a continuous distribution of adduct from  $q_o^i$  to  $q_{\text{max}}^i$ . Here  $q_{\text{max}}^i$  signifies some  $q^i$  at a suitably high level above the highest exit channel (the index  $q_{\text{min}}^i$ , which distinguished the activated from stabilized adducts in the chemical activation analysis is irrelevant here). The eigenvector  $g_i^q$ , which describes the shape-invariant population distribution, is found through the equation

$$\omega \sum_r P_{i_r}^{qr} g_i^r - (k_i^q + \omega) g_i^q = -k_i^{\text{uni}} g_i^q \quad (\text{MEM13})$$

where the differential sum of output rate constants is given by

$$k_i^q = \sum_p d_{p,i}^q \quad (\text{MEM14})$$

Despite appearances, (MEM14) is identical to the equation in (A2) since isomerizations are now considered product channels. The rate constant to any product channel, including a stabilized isomer, is found by summing the product of the differential rate constant and the (normalized) distribution function,

$$k_p^{\text{prod}} = \frac{\sum_q d_{p,i}^q g_i^q}{\sum_q g_i^q} \quad (\text{MEM15})$$

where the sum in the denominator is over all  $q$ . In the notation of the Appendix, the eigenvalue problem is expressed

$$\bar{J}'_i \bar{g}_i = -k_i^{\text{uni}} \bar{g}_i \quad (\text{MEM16})$$

Here  $\bar{J}'_i$  is essentially  $-\bar{J}_{11}$  of eq A3. All eigenvectors represent profiles, which decay exponentially with time with decay rates proportional to their eigenvalues. That eigenvector which corresponds to the slowest decay rate is the asymptotic solution and the only eigenvector that needs to be found. The equation is solved using a successive iteration scheme in which the high-pressure result is used as the initial guess for  $\bar{g}_i$ . The procedure follows closely that described in Gilbert and Smith and needs no additional elaboration.

#### Modified Strong-Collision Model for Chemical Activation.

In the modified strong collision approximation, collision stabilization is assumed to occur via a single-step process. A collision either stabilizes an activated complex completely or leaves it unchanged. The modified strong collision model is essentially a modification of the strong collision limit in which the standard Lennard-Jones collision frequency is multiplied by a stabilization efficiency factor  $\beta_c$ .

As before, the chemical activation problem considers a single input channel, which can form various products through multiple isomerizations. The rate constants to form products and stabilized adducts are again defined by (MEM1) and (MEM2). In the modified strong collision approximation, the steady-state analysis of (MEM3) is replaced by

$$f_i^q + \sum_j k_{ij}^q n_j^q = n_i^q \left( \sum_p d_{p,i}^q + \sum_j k_{ji}^q + \beta_c \omega \right) \quad (\text{MEM17})$$

In the absence of collisional energy redistribution, there is no coupling between energy levels. (MEM17) represents a simple matrix equation (in isomer space) that is solved at each energy

level for the vector describing the population distribution among isomers. Once this is obtained for all  $E$ , the overall rate constant to products are obtained by (MEM4). The rate constant to form stabilized adducts is given by

$$k_i^{\text{stab}}(T,P) = \beta_c \omega \sum_r n_i^r \quad (\text{MEM18})$$

which is used in place of (MEM5). The calculation is sensitive to the collision efficiency  $\beta_c$ , which, if ideally chosen, connects the results of the modified strong collision analysis to the master equation solution. The method for assigning  $\beta_c$  is described in ref 31.

(MEM17) is solved independently for each energy level beginning at that level corresponding to the input barrier (in the modified strong collision assumption, levels below this can never be occupied). The solution of (MEM17) is calculated for increasing values of energy until a convergence criterion on a level above the highest exit channel is satisfied. For expediency, the problem can be constructed to solve several temperature and pressure cases simultaneously, with loops arranged in the order (outer to inner): energy; temperature, and pressure. This greatly diminishes the degree of redundant calculation and required storage. Provision has to be made for cases where a high barrier to isomerization prevents any population from reaching an isomeric subsystem at low energies. These cases produce singular matrices and some logic has to be incorporated to identify and remove inactive isomers from the calculation at these energies.

**Modified Strong Collision Model for Dissociation.** In the modified strong collision dissociation model, a single collision is assumed to transform a stabilized molecule to an activated one with probability  $\beta_c$ . This clear distinction between stabilized and activated molecules makes this dissociation model nearly analogous to the modified strong collision chemical activation model. In fact, (MEM17), which was defined for chemical activation, can be used directly for dissociation with the simple replacement of the source function  $f_i^q$ .

In the modified strong collision approximation, an expression for the source function is obtained by performing a detailed balance comparison of the rate constants of collisional activation and stabilization in the high-pressure limit. This relates  $f_i^q$  to the equilibrium population distribution and the effective collision frequency,

$$f_i^q = \beta_c \omega \frac{\rho_c(E_q) e^{-E_q/RT}}{\sum_q \rho_c(E_q) e^{-E_q/RT}} \delta_{im} \quad (\text{MEM19})$$

where  $m$  denotes the dissociating isomer.

With the substitution of (MEM19), (MEM17) can be solved as described in the previous section. For each initial dissociating isomer  $e$ , rate constants to products and stabilized adducts are again defined via (MEM12) (replacing the subscript  $i$  by  $m$ ), except in this case the analysis includes the effect of multiple isomerization. Rate constants are obtained from every dissociating isomer to all product channels and stabilized adducts in the system, not just those directly accessible to that isomer. This is in stark contrast to the master equation analysis in which a time-independent solution of the multiple isomerization dissociation problem was not possible.

**Mechanism Construction.** To apply the results of the chemical activation and the thermal dissociation analysis for comparison to data, it is necessary to construct an elementary

chemical reaction mechanism. The mechanism includes all the reactions involved in the chemical activation process, including stabilizations and reactions for thermal dissociation of the stabilized species. Reactions are reversible, so that we implicitly account for some of the thermal dissociation reactions as the reverse of the forward (chemically activated) reactions; e.g., CH<sub>3</sub>CH<sub>2</sub>OO• dissociation to C<sub>2</sub>H<sub>5</sub> + O<sub>2</sub> is included as the reverse of C<sub>2</sub>H<sub>5</sub> + O<sub>2</sub> ⇌ CH<sub>3</sub>CH<sub>2</sub>OO•. Thermal dissociation to products (other than the original reactants C<sub>2</sub>H<sub>5</sub> + O<sub>2</sub>) must be specifically included. We also needed to include other reactions for analysis of the experiments considered in this work, to account for competing processes, such as HO<sub>2</sub> + HO<sub>2</sub>, .... We used the same reactions used in the experimental analysis.

Since the QRRK rate coefficients are dependent on both temperature and pressure, the conventional approach is to use different sets of rate coefficients at each pressure. An alternative approach is to use Chebyshev polynomials to represent a rate constant expression as a function of both temperature and pressure, as described by Venkatesh et al.<sup>19,20</sup> The temperature–pressure dependent rate coefficients in Chebyshev format for the current system of interest is derived from application of the methodology described by Venkatesh et al. The current mechanism files are derived on the basis of seven temperature functions and three pressure functions to fit the rate coefficients over a 50 × 50 Gauss-Chebyshev grid using a Levenberg–Marquardt algorithm. The current mechanism file is fitted over a temperature range of 250–1200 K and a pressure range of 10<sup>−3</sup> to 100 atm. Refer to Supporting Information Tables 1 and 2 for the C<sub>2</sub>H<sub>5</sub> + O<sub>2</sub> mechanism file, in Chebyshev polynomial format, used in this study. The CHEMKIN integrator package program<sup>21</sup> has been modified to accept rate coefficients in the Chebyshev format. The idea of having a single CHEMKIN mechanism file capable of determining concentration profiles over a wide temperature and pressure range is appealing; however, the Chebyshev polynomials are still fitted parameters and verification of calculated rate constants should be checked for consistency.

## Results and Discussion

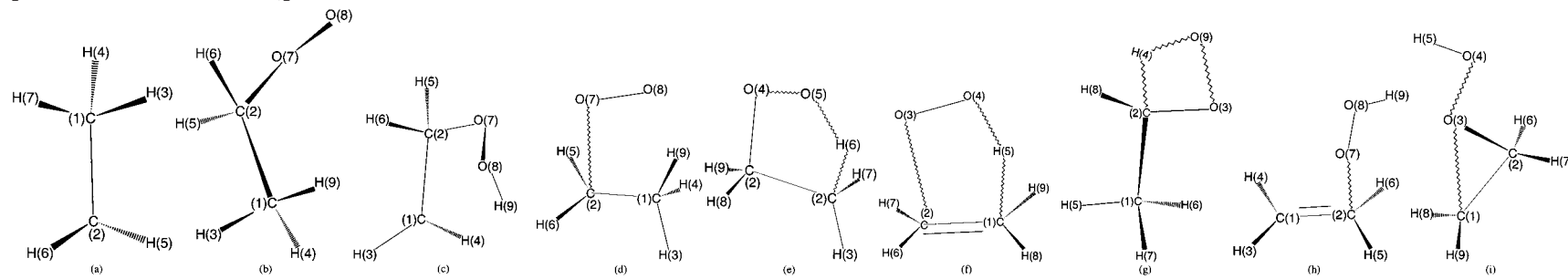
**Geometries.** Optimized geometric structures for the reactants, transition states, adducts, and products are calculated at the B3LYP/6-31G(d,p) level of theory and are listed in Table 1. Table 2 lists the unscaled vibrational frequencies and moments of inertia. Comparison of geometric parameters calculated by Rienstra-Kiracofe et al (hereafter denoted as RKAS) at the high level coupled cluster ab initio method are presented in {braces}.<sup>17</sup>

The TS for molecular elimination of ethylene from the ethylperoxy radical (denoted as TS1 in Figure 2) has a C–C bond of 1.38 Å {1.39 Å}, considerably shorter than the normal C–C bond length of approximately 1.53 Å and slightly longer than the normal C=C bond of 1.34 Å. The C–O bond is 2.20 Å {2.14 Å}, approximately 0.8 Å longer than the normal C–O bond length. Shortening of the O–O bond to 1.28 Å {1.29 Å} is also observed. The O–H bond length is 1.25 Å {1.26 Å} and the C–H bond is 1.38 Å {1.36 Å}. The spin contamination, ⟨S<sup>2</sup>⟩, is 0.76, which is consistent with the spin for a doublet.

The TS for isomerization of CH<sub>3</sub>CH<sub>2</sub>OO• to •CH<sub>2</sub>CH<sub>2</sub>OOH is a five-member ring (denoted as TS2). The oxygen–hydrogen bond length is 1.19 Å {1.23 Å} and the carbon–hydrogen bond is 1.40 Å {1.35 Å}, both slightly longer than the stable O–H bond length, ca. 0.96 Å, and the C–H bond length, ca. 1.08 Å. The spin contamination is slightly higher than that of TS1 with ⟨S<sup>2</sup>⟩ = 0.81.

The TS for β-scission of •CH<sub>2</sub>CH<sub>2</sub>OOH to ethylene + HO<sub>2</sub> (denoted as TS3) shows a C–C bond of 1.38 Å {1.39 Å} and

TABLE 1: Optimized Geometric Parameters for Species in the Ethyl + O<sub>2</sub> Oxidation System at the B3LYP/6-31G(d,p) Level of Theory and Geometric Parameters of Transition States Optimized at B3LYP/6-31G(d,p)<sup>a</sup>



C <sub>2</sub> H <sub>5</sub>		CH <sub>3</sub> CH <sub>2</sub> OO•		•CH <sub>2</sub> CH <sub>2</sub> OOH		TS[C <sub>2</sub> H <sub>5</sub> -O <sub>2</sub> ]		TS2		TS1		TS5		TS3		TS4	
Parameter	Value	Parameter	Value	Parameter	Value	Parameter	Value	Parameter	Value	Parameter	Value	Parameter	Value	Parameter	Value	Parameter	Value
r21	1.4886	r21	1.5174	r21	1.4867	r21	1.4787	r21	1.5256	r21	1.3849	r21	1.5009	r21	1.3792	r21	1.4753
r31	1.1041	r31	1.0944	r31	1.0839	r31	1.0953	r31	1.0884	r32	2.2040	r32	1.3927	r31	1.0848	r32	1.3996
r41	1.0959	r41	1.0936	r41	1.0857	r41	1.0953	r42	1.4341	r43	1.2778	r42	1.3314	r41	1.0848	r43	1.7530
r52	1.0848	r52	1.0935	r52	1.1028	r52	1.0842	r54	1.4231	r54	1.2480	r51	1.0936	r52	1.0857	r54	0.9722
r62	1.0848	r62	1.0932	r62	1.0964	r62	1.0842	r65	1.1925	r62	1.0843	r61	1.0931	r62	1.0859	r62	1.0953
r71	1.0959	r72	1.4625	r72	1.4338	r72	1.2245	r71	1.0903	r72	1.0843	r71	1.0982	r72	1.9080	r72	1.0958
a312	112.1	r87	1.3231	r87	1.4545	r91	1.1090	r82	1.0971	r81	1.0888	r82	1.0958	r87	1.3932	r81	1.0827
a412	111.9	r91	1.0926	r98	0.9715	a312	112.2	r92	1.0958	r91	1.0888	r94	1.2736	r98	0.9744	r91	1.0828
a521	120.9	a312	109.9	a312	121.6	a412	112.2	a312	118.4	a321	96.8	a321	115.8	a312	121.1	a321	83.0
a621	120.9	a412	111.0	a412	119.7	a521	121.3	a421	104.2	a432	98.2	a421	114.1	a412	121.2	a432	107.3
a712	111.9	a521	112.6	a521	111.6	a621	121.3	a542	102.3	a543	98.8	a512	111.0	a521	119.6	a543	93.2
d4123	-119.3	a621	112.4	a621	111.8	a721	91.3	a654	94.4	a621	121.8	a612	110.5	a621	119.5	a621	115.6
d5213	85.1	a721	111.0	a721	113.5	a872	103.4	a712	116.4	a721	121.8	a712	109.9	a721	105.4	a721	116.5
d6213	-85.0	a872	111.0	a872	107.1	a912	110.9	a821	110.4	a812	118.8	a821	118.7	a872	110.4	a812	120.1
d7123	119.3	a912	109.9	a987	100.6	d4123	-122.7	a921	114.8	a912	118.8	a942	102.7	a987	103.0	a912	120.5
		d4123	-120.0	d4123	-175.6	d5213	152.1	d4213	-144.6	d4321	0.0	d4213	-96.6	d4123	-171.9	d4321	171.9
		d5213	64.4	d5213	107.5	d6213	-29.2	d5421	45.7	d5432	0.0	d5123	172.5	d5213	-17.1	d5432	-139.0
		d6213	-60.1	d6213	-13.4	d7213	241.4	d6542	-34.1	d6213	94.8	d6123	50.9	d6213	-169.3	d6213	113.1
		d7213	179.9	d7213	-138.3	d8721	-0.1	d7123	-142.7	d7123	-94.7	d7123	-68.0	d7213	85.0	d7213	-113.6
		d8721	71.2	d8721	70.8	d9123	118.6	d8213	-25.5	d8126	-10.8	d8213	140.0	d8721	84.0	d8123	-86.4
		d9123	119.5	d9872	-100.1	r72	2.8625	d9213	99.4	d9126	-159.7	d9421	118.8	d9872	82.9	d9123	84.6

<sup>a</sup> Key for the ethyl + O<sub>2</sub> oxidation system: (a) ethyl radical; (b) ethylperoxy radical; (c) ethylhydroperoxy. Key for the transition states: (d) C<sub>2</sub>H<sub>5</sub> + O<sub>2</sub> → CH<sub>3</sub>CH<sub>2</sub>OO•; (e) CH<sub>3</sub>CH<sub>2</sub>OO• → •CH<sub>2</sub>CH<sub>2</sub>OOH; (f) C<sub>2</sub>H<sub>5</sub> + O<sub>2</sub> → C<sub>2</sub>H<sub>4</sub> + HO<sub>2</sub>; (g) CH<sub>3</sub>CH<sub>2</sub>OO• → CH<sub>3</sub>CHO + OH; (h) •CH<sub>2</sub>CH<sub>2</sub>OOH → C<sub>2</sub>H<sub>4</sub> + HO<sub>2</sub>; (i) •CH<sub>2</sub>CH<sub>2</sub>OOH → oxirane + OH. Parameters: r corresponds to atomic distance between respective atoms in Angstroms, a is the bond angle in degrees, and d is the dihedral angle in degrees.

**TABLE 2: Vibrational Frequencies (cm<sup>-1</sup>) for Species in the Ethyl Oxidation System Calculated at the B3LYP/6-31G(d,p) Level of Theory<sup>a</sup>**

species	frequencies								moment of inertia (GHz)
C <sub>2</sub> H <sub>5</sub> ( <b>1a</b> )	122.2	464.0	813.7	984.0	1071.2	1198.9	1412.8	1480.8	103.49857
	1496.4	3102.3	3160.8	3262.3	1496.9	2963.7	3056.1		22.68020
CH <sub>3</sub> CH <sub>2</sub> OO• ( <b>1b</b> )	113.5	236.1	358.1	528.8	801.8	849.5	1000.9	1102.4	17.64590
	1163.2	1209.2	1309.4	1381.0	1419.6	1493.8	1499.6	1519.1	5.64663
	3059.1	3077.3	3129.1	3136.1	3154.3				4.86165
•CH <sub>2</sub> CH <sub>2</sub> OOH ( <b>1c</b> )	132.5	163.0	221.1	359.3	461.4	559.1	841.6	872.3	16.07642
	965.6	1067.3	1141.4	1273.5	1364.6	1379.3	1459.4	1476.5	5.74828
TS[C <sub>2</sub> H <sub>5</sub> -O <sub>2</sub> ] ( <b>1d</b> )	2987.1	3069.9	3160.7	3272.1	3745.4				4.86523
	87.4(i)	81.2	147.8	153.1	226.6	252.9	560.6	822.6	14.30872
	974.0	1081.9	1200.5	1409.8	1481.4	1491.2	1502.7	1564.8	3.49729
TS2 ( <b>1e</b> )	2907.8	3060.6	3112.4	3171.7	3274.4				2.91838
	2227.4(i)	277.1	436.7	551.3	688.3	873.0	905.5	913.2	13.80300
	970.2	1050.3	1108.4	1170.7	1247.2	1350.5	1467.8	1509.6	7.73280
TS1 ( <b>1f</b> )	1737.6	3038.3	3097.6	3120.8	3216.3				5.62039
	1069.9(i)	216.4	365.8	474.2	523.9	628.1	833.1	897.0	14.67621
	1004.8	1038.1	1229.6	1295.4	1327.1	1356.2	1480.0	1586.7	5.59606
TS5 ( <b>1g</b> )	1626.8	3124.2	3179.8	3205.1	3270.2				4.28511
	1832.6(i)	129.1	207.7	414.7	657.1	783.5	818.5	919.2	20.56639
	1065.6	1119.6	1129.6	1171.0	1366.6	1418.5	1487.8	1493.9	5.17032
TS3 ( <b>1h</b> )	1965.5	3032.7	3078.7	3107.4	3144.7				4.84130
	526.5(i)	79.9	218.9	299.8	427.3	457.1	815.2	830.4	17.77077
	930.5	1020.1	1068.0	1244.8	1271.0	1388.6	1475.5	1564.9	4.32924
TS4 ( <b>1i</b> )	3150.6	3167.3	3232.9	3266.5	3674.5				4.04617
	765.0(i)	79.3	125.1	256.2	399.2	504.7	756.7	837.9	26.63204
	938.0	1011.8	1171.9	1178.7	1203.8	1317.5	1483.0	1550.3	4.48611
	3043.2	3099.6	3187.6	3305.2	3776.8				4.08337

<sup>a</sup> The frequencies reported are not scaled. Imaginary frequencies are denoted by "(i)".

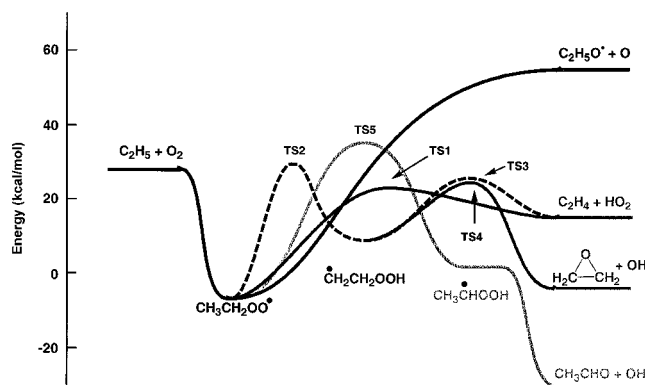


**Figure 2.** Potential energy diagram for the C<sub>2</sub>H<sub>5</sub> + O<sub>2</sub> system calculated at CBS-Q//B3LYP/6-31G(d,p).

a C–O bond length of 1.91 Å {1.93 Å}. This is also described by Chen and Bozzelli.<sup>38</sup> The TS for the formation of the oxirane + OH products from the hydroperoxyethyl adduct (denoted as TS4) has a C–O bond length of 1.40 Å {1.41 Å} and an O–C bond of 1.91 Å {1.94 Å}. The dissociating O–O bond is 1.75 Å {1.77 Å}. Spin contamination for TS3 is 0.78 and for TS4 is 0.81.

The TS for the formation of the acetaldehyde + OH from the CH<sub>3</sub>CH<sub>2</sub>OO• adduct via a four-member ring isomerization on the ipso-carbon (denoted as TS5) shows a C–H bond length 1.33 Å {1.32 Å} and an O–H bond length of 1.27 Å {1.27 Å}. The O–O bond length is 1.50 Å {1.54 Å}, slightly longer than the normal O–O bond length of 1.46 Å. Spin contamination for TS5 calculated by B3LYP/6-31G(d,p) is 0.76.

Comparison of the bond lengths for the transition states in this system calculated at the B3LYP/6-31G(d,p) level of theory with the values determined by RKAS using coupled cluster theory are typically within 0.02 Å, with the largest difference at 0.06 Å.

The TS for the O<sub>2</sub> + C<sub>2</sub>H<sub>5</sub> ⇌ [CC–OO]‡ ⇌ CH<sub>3</sub>CH<sub>2</sub>OO• reaction does not exhibit any barrier for the addition reaction, and therefore, one cannot utilize the saddle point requirement for TS calculations. The reaction coordinate for this reaction is determined by incremental increases in the C–O bond distance along the dissociation reaction path, starting with the full geometrically optimized ethylperoxy radical at the B3LYP/6-31G(d,p) level of theory. (Refer to Figure 1.) Calculations are performed over the C–O bond length range of 1.46–4.46 Å in an incremental step size of 0.10 Å. Each of the geometric configurations of the “stretched” ethylperoxy radical are fully optimized, with respect to the constraint of the “frozen” C–O bond distance of interest. The spin contamination for the ethyl radical and the CH<sub>3</sub>CH<sub>2</sub>OO• radical are 0.75. Spin contamination also begins to deviate from the theoretical spin for a doublet at C–O bond lengths above 2.0 Å. The spin contamination at 2.0 Å is 0.87, which is slightly higher than the theoretical spin of 0.75 for a doublet. A steady linear increase in the spin contamination value is observed as the C–O bond length is increased from 2.0 to 3.4 Å; i.e., for every 0.1 Å increase in the C–O bond length, an increase of 0.06 in ⟨S<sup>2</sup>⟩ is observed. The spin contamination at 3.4 Å is 1.7.

**Thermodynamic Properties: Δ<sub>f</sub>H<sub>298</sub>, S<sub>298</sub>, and C<sub>p</sub>(300–1500 K).** Thermodynamic properties used in the current study are presented in Table 3. Enthalpy of formation and entropy values are reported at 298 K, as most experimental data are referenced or available at 298 K. This facilitates the use of these thermodynamic properties and the use ofisodesmic reaction sets. Total energies calculated by ab initio and DFT methods are presented in Supporting Information Table 3. Entropy and heat capacities are calculated by statistical mechanics, as outlined above. Pitzer-Gwinn’s<sup>29</sup> general treatment of hindered internal rotational contributions is used to adjust for entropy and C<sub>p</sub> values. (Refer to Supporting Information Table 4 for rotational barriers and hindered moments of inertia used in the Pitzer-Gwinn treatment). Entropy and heat capacity for the association



**TABLE 3: Thermodynamic Properties of Species in the Ethyl Oxidation System Calculated at CBS-Q//B3LYP/6-31G(d,p)**

species <sup>a</sup>	$\Delta_f H_{298}^\circ$	$S_{298}^\circ$	$C_p(300)$	$C_p(400)$	$C_p(500)$	$C_p(600)$	$C_p(800)$	$C_p(1000)$	$C_p(1500)$
C <sub>2</sub> H <sub>5</sub>	28.6	60.61	12.20	14.64	17.01	19.11	22.62	25.39	29.96
O <sub>2</sub>	0	49.01	7.02	7.23	7.44	7.65	8.04	8.35	8.73
CH <sub>3</sub> CH <sub>2</sub> OO•	-6.72	73.82	16.20	19.86	23.34	26.36	31.11	34.63	40.08
TS1	23.76	70.76	17.47	21.62	25.25	28.26	32.82	36.05	40.94
TS2	29.64	68.83	16.38	20.91	24.82	28.01	32.77	36.1	41.04
•CH <sub>2</sub> CH <sub>2</sub> OOH	11.22	81.91	20.25	23.52	26.36	28.72	32.30	35.13	39.67
TS3	27.07	79.06	19.38	22.73	25.55	27.85	31.35	34.11	38.61
TS4	26.51	77.46	19.04	22.52	25.54	28.03	31.86	34.74	39.43
TS5	35.04	73.07	16.99	20.83	24.31	27.26	31.80	35.09	40.03
C <sub>2</sub> H <sub>4</sub>	12.52	52.47	10.2	12.72	15.02	17	20.14	22.54	26.38
HO <sub>2</sub>	3.8	54.73	8.37	8.95	9.48	9.96	10.78	11.43	12.47
oxirane	-12.57	59.35	11.3	14.74	17.9	20.55	24.57	27.46	
OH	9.49	43.88	7.16	7.08	7.05	7.05	7.15	7.33	7.87
CH <sub>3</sub> CHO	-39.18	63.13	13.22	15.71	18.22	20.47	24.22	26.97	

<sup>a</sup> The notation correlates to the structure shown in Table 1.

**TABLE 4: Enthalpy of Formation for the Two Adducts in This System, Methylperoxy Radical and Methyl Hydroperoxide Molecule, Determined from the Use of Isodesmic Reaction Sets**

isodesmic reaction				$\Delta H_f$ (kcal mol <sup>-1</sup> )	method		
CH <sub>3</sub> CH <sub>2</sub> OOH	+	CH <sub>3</sub> OH <sup>a</sup>	=	CH <sub>3</sub> CH <sub>2</sub> OH <sup>a</sup>	+ CH <sub>3</sub> OOH <sup>b,c</sup>	-39.9 ± 1.5	CBS-Q//B3LYP/6-31G(d,p)
		-48.0 ± 0.05		-56.2 ± 0.12	-31.8 ± 0.94		
CH <sub>3</sub> CH <sub>2</sub> OOH	+	CH <sub>3</sub> OH <sup>a</sup>	=	CH <sub>3</sub> CH <sub>2</sub> OH <sup>a</sup>	+ CH <sub>3</sub> OOH <sup>b,c</sup>	-40.1 ± 1.8	G2
		-48.0 ± 0.05		-56.2 ± 0.12	-31.8 ± 0.94		
CH <sub>3</sub> CH <sub>2</sub> OO•	+	CH <sub>3</sub> OOH <sup>b,c</sup>	=	CH <sub>3</sub> OO• <sup>c,d</sup>	+ CH <sub>3</sub> CH <sub>2</sub> OOH	-6.7 ± 2.3	CBS-Q//B3LYP/6-31G(d,p)
		-31.8 ± 0.94		2.15 ± 0.91	-39.89 ± 1.54		
CH <sub>3</sub> CH <sub>2</sub> OO•	+	CH <sub>3</sub> OOH <sup>b,c</sup>	=	CH <sub>3</sub> OO• <sup>c,d</sup>	+ CH <sub>3</sub> CH <sub>2</sub> OOH	-6.8 ± 2.7	G2
		-31.8 ± 0.94		2.15 ± 0.91	-40.06 ± 1.78		
•CH <sub>2</sub> CH <sub>2</sub> OOH	+	CH <sub>3</sub> CH <sub>2</sub> OH <sup>a</sup>	=	CH <sub>3</sub> CH <sub>2</sub> OOH	+ CH <sub>2</sub> •CH <sub>2</sub> OH <sup>e</sup>	11.2 ± 2.1	CBS-Q//B3LYP/6-31G(d,p)
		-56.23 ± 0.12		-39.89 ± 1.54	-5.70 ± 0.85		
•CH <sub>2</sub> CH <sub>2</sub> OOH	+	CH <sub>3</sub> OH <sup>a</sup>	=	CH <sub>3</sub> CH <sub>2</sub> OOH	+ C•H <sub>2</sub> OH <sup>f</sup>	10.5 ± 2.4	G2
		-48.07 ± 0.05		-40.06 ± 1.78	-3.5 ± 0.7		
CH <sub>3</sub> OOH	+	H <sub>2</sub> O <sup>g</sup>	=	HOOH <sup>h</sup>	+ CH <sub>3</sub> OH <sup>a</sup>	-30.8 ± 0.7	CBS-APNO
		-57.8 ± 0.01		-32.53	-48 ± 0.05		
CH <sub>3</sub> OOH	+	CH <sub>3</sub> CH <sub>3</sub> <sup>a</sup>	=	CH <sub>3</sub> OH <sup>a</sup>	+ CH <sub>3</sub> CH <sub>2</sub> OH <sup>a</sup>	-30.8 ± 0.7	CBS-APNO
		-20.04 ± 0.07		-48 ± 0.05	-56.23 ± 0.12		
CH <sub>3</sub> OOH	+	CH <sub>4</sub> <sup>i</sup>	=	CH <sub>3</sub> OH <sup>a</sup>	+ CH <sub>3</sub> OH <sup>a</sup>	-30.4 ± 0.7	CBS-APNO
		-17.8 ± 0.1		-48 ± 0.05	-48 ± 0.05		
CH <sub>3</sub> OO•	+	CH <sub>3</sub> OH <sup>a</sup>	=	CH <sub>3</sub> O• <sup>j</sup>	+ CH <sub>3</sub> OOH	-30.67 ± 1.23	arithmetic mean value
		-48 ± 0.05		4.1 ± 1.0	-30.67 ± 1.23	1.2 ± 1.7	CBS-APNO
CH <sub>3</sub> OO•	+	CH <sub>3</sub> CH <sub>2</sub> OH <sup>a</sup>	=	CH <sub>3</sub> CH <sub>2</sub> O• <sup>k</sup>	+ CH <sub>3</sub> OOH	0.3 ± 2.4	CBS-Q//B3LYP/6-31G(d,p)
		-56.23 ± 0.12		-3.9 ± 1.27	-30.67 ± 1.23		

<sup>a</sup> Green, J. H. S. Revision of the values of the heats of formation of normal alcohols. *Chem. Ind.* **1960**, 1215. NIST webbook: <http://webbook.nist.gov/>. <sup>b</sup> Lay, T. S.; Bozzelli, J. W. *J. Phys. Chem. A* **1997**, **101**, 9505. <sup>c</sup> Sun, H.; Chen, C-J.; Bozzelli, J. W. *J. Phys. Chem. A* **2000**, **104**, 8270. <sup>d</sup> Knyazev, V. D.; Slagle, I. R. *J. Phys. Chem. A* **1998**, **102**, 1770. <sup>e</sup> Sun, H.; Bozzelli, J. W. *J. Phys. Chem. A* **2001**, **105**, 9543. <sup>f</sup> Based on the CBS-APNO calculated value and: Walch, S. P. *J. Chem. Phys.* **1993**, **98**, 3163. <sup>g</sup> Cox, Wagner, et al., 1984. NIST webbook: <http://webbook.nist.gov/>. <sup>h</sup> Chase, 1998, JANAF. NIST webbook: <http://webbook.nist.gov/>. <sup>i</sup> Pittam and Pilcher, 1972. NIST webbook: <http://webbook.nist.gov/>. <sup>j</sup> Tsang, W., 1996. NIST webbook: <http://webbook.nist.gov/>. <sup>k</sup> Sun, H.; Chen, C-J.; Bozzelli, J. W. *J. Phys. Chem. A* **2002**, **106**, 3947.

TS is also determined from statistical mechanics with scaled frequencies and moments of inertia from each C–O configuration. However, as the C–O bond distance increases, the C–O rotor becomes more of a free-rotor. This difficulty in determining the “changing” contribution is not addressed, but instead the same hindered rotor entropy and  $C_p$  contribution used in the stable adduct is utilized in the hindered rotor contribution to  $S$  and  $C_p$  for the VTST structure species. The hindered rotor contribution for both the ethylperoxy adduct and VTST structures at 298 K for entropy is 12.09 cal mol<sup>-1</sup> K<sup>-1</sup> and for  $C_p$  is 3.28 cal mol<sup>-1</sup> K<sup>-1</sup>.

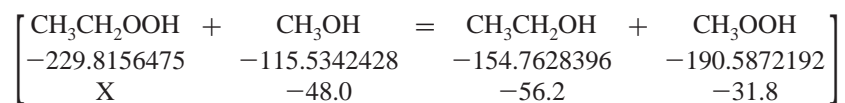
The enthalpy of formation for reactants, TS, adducts, and products are calculated at the CBS-Q//B3LYP/6-31G(d,p) level of theory. The enthalpy of formation for the ethyl radical is well-known and generally accepted to be 28.5 ± 0.5 kcal mol<sup>-1</sup>,<sup>39</sup> and Marshall recently performed high level ab initio calculations at CCSD(T) level of theory and reports 28.8 ± 0.5

kcal mol<sup>-1</sup>.<sup>40</sup> The enthalpy of formation for the ethyl radical used in this study is 28.6 kcal mol<sup>-1</sup>.

**Adduct Enthalpy of Formation.** Isodesmic reaction analyses are performed on the two adducts in this system, i.e., ethylperoxy and the hydroperoxyethyl radical, at three different levels of calculation. The composite ab initio methods utilized are the CBS-Q//B3LYP/6-31G(d,p) and G2 levels of calculation. The following illustrates the typical approach utilizing isodesmic reactions to obtain enthalpy of formation values. Two sets of isodesmic reactions are used to determine the enthalpy of formation for the ethylperoxy radical at the CBS-Q//B3LYP/6-31G(d,p) level of theory in Scheme 1.

The  $\Delta_f H_{298}$  for the ethylperoxy radical, determined by use of isodesmic reactions is -6.7 kcal mol<sup>-1</sup>. This value is in very good agreement with recent publications<sup>9-11,13,41</sup> and results in a well depth for ethyl + O<sub>2</sub> to ethylperoxy radical of 35.3 kcal mol<sup>-1</sup>.

## SCHEME 1

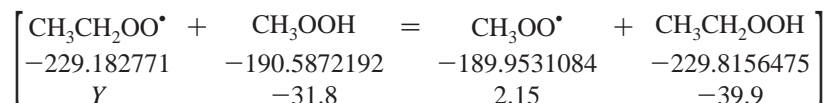


$$\Delta E \text{ (hartrees)} = [(-154.7628396) + (-190.5872192)] - [(-229.8156475) + (-115.5342428)]$$

$$= -0.000168562 \text{ hartrees} = -0.11 \text{ kcal mol}^{-1}$$

$$\Delta H_{\text{rxn}} = -0.11 \text{ kcal mol}^{-1} = [(-31.8) + (-56.2)] - [(-48) + X]$$

$$X = -39.9 \text{ kcal mol}^{-1}$$



$$\Delta E \text{ (hartrees)} = [(-189.9531084) + (-229.8156475)] - [(-229.182771) + (-190.5872192)]$$

$$= 0.001234314 \text{ hartrees} = 0.77 \text{ kcal mol}^{-1}$$

$$\Delta H_{\text{rxn}} = 0.77 \text{ kcal mol}^{-1} = [(2.15) + (-39.89)] - [(-31.8) + Y]$$

$$Y = -6.7 \text{ kcal mol}^{-1}$$

Comparison of the two radicals with the different methods of calculation shows that both CBS-Q//B3LYP/6-31G(d,p) and G2 are similar and agree with values reported in the literatures. The difference in energy between G2 and those from literature is less than 0.5 kcal mol<sup>-1</sup>. The CBS-Q analysis is used (as opposed to G2) because of significantly lower spin contamination and slightly lower error limits.

The calculated enthalpy of formation results from use of isodesmic reactions are shown in Table 4. The values for the ethylperoxy radical calculated at the CBS-Q//B3LYP/6-31G(d,p) and at G2 levels of theory show similar results, -6.7 and -6.8 kcal mol<sup>-1</sup>, respectively. The recent study of Blanksby et al. reports a value of -6.8 ± 2.3 kcal mol<sup>-1</sup> for the ethylperoxy radical and -39.7 kcal mol<sup>-1</sup> for ethyl hydroperoxide, which are in good agreement with the values in Table 4.<sup>42</sup>

A value of ethylperoxy radical can also be estimated from the Δ<sub>f</sub>H<sub>298</sub> of ethyl radical (28.6 kcal mol<sup>-1</sup>) and the well depth of 31.5 kcal mol<sup>-1</sup> reported by RKAS<sup>17</sup> (adjusted for thermal energy in this study) results in a value that is -2.9 kcal mol<sup>-1</sup> for the ethylperoxy radical, ca. 4 kcal mol<sup>-1</sup> higher than the values above.

The calculated value of 11.2 kcal mol<sup>-1</sup> for hydroperoxyethyl radical at CBS-Q//B3LYP/6-31G(d,p) is in agreement with the CBS-q//B3LYP/6-31G(d) value of 11.3 kcal mol<sup>-1</sup> published by Chen and Bozzelli.<sup>38</sup> The same isodesmic reactions at the G2 level of theory result in a value of 10.5 kcal mol<sup>-1</sup>.

Inspection of Scheme 1 above shows that our Δ<sub>f</sub>H<sub>298</sub> values for the ethylperoxy radical and ethyl hydroperoxide are closely tied to Δ<sub>f</sub>H<sub>298</sub> values of both methyl hydroperoxide and the methylperoxy radical, and we evaluate this. Propagation of the uncertainty limits, including contribution from the ab initio method, i.e., CBS-Q and G2, has also been taken into consideration. The uncertainty level corresponding to the ab initio method, based on 1 standard deviation for the root-mean-square analysis, are 1.2 and 1.5 kcal mol<sup>-1</sup>, respectively.<sup>22</sup> The uncertainty limits resulting from the isodesmic reaction set calculations for the ethylperoxy and ethylhydroperoxy radicals are shown in Table 4.

Literature values for the enthalpy of formation for the methyl-hydroperoxide molecule and methylperoxy radical vary by over 4 kcal mol<sup>-1</sup>. Blanksby et al.<sup>42</sup> have tabulated available

literature sources of Δ<sub>f</sub>H<sub>298</sub> for both the CH<sub>3</sub>OO• radical and CH<sub>3</sub>OOH molecule; for the CH<sub>3</sub>OO• radical the Δ<sub>f</sub>H<sub>298</sub> ranges from 1.0 to 6.3 kcal mol<sup>-1</sup> and for CH<sub>3</sub>OOH from -30.2 to -34.6 kcal mol<sup>-1</sup>. Blanksby et al. report their findings on these two species and report their best value for CH<sub>3</sub>OO• to be 4.8 ± 1.2 kcal mol<sup>-1</sup> and for CH<sub>3</sub>OOH to be -30.9 ± 0.7 kcal mol<sup>-1</sup>, within the range of the reported literature values.

We further calculate Δ<sub>f</sub>H<sub>298</sub> of CH<sub>3</sub>OOH using the CBS-APNO method and three working reactions that do not have group balance and are, therefore, not derived from the methylperoxy radical; reactions are listed in Table 4. Values obtained are -30.8, -30.8, and -30.4 kcal mol<sup>-1</sup>. Sun et al.<sup>43</sup> also report calculated values of -30.9, -31.6, and -31.3 kcal mol<sup>-1</sup> using CBS-Q level of theory. These values and the value of Blanksby et al are in good agreement.

The noted good agreement between different studies for ethyl hydroperoxide, methyl hydroperoxide, and the ethylperoxy radical suggests that we should be able to use these species and their Δ<sub>f</sub>H<sub>298</sub> values in group balance isodesmic reactions to further evaluate the Δ<sub>f</sub>H<sub>298</sub> of the methylperoxy radical. Use of -6.7 kcal mol<sup>-1</sup> for ethylperoxy, -30.7 kcal mol<sup>-1</sup> for methyl hydroperoxide, and -39.8 kcal mol<sup>-1</sup> for ethyl hydroperoxide result in values of ca. 1.2 kcal mol<sup>-1</sup> for the methylperoxy radical. This is the same value we obtain with a working reaction in Table 4 and CBS-APNO calculations. These values for methylperoxy are some 3.6 kcal mol<sup>-1</sup> below the value recommended by Blanksby et al. Brinks et al.<sup>44</sup> report a value of methylperoxy of 0 from G2 calculations, when Δ<sub>f</sub>H<sub>298</sub> of 35 kcal mol<sup>-1</sup> is used for the CH<sub>3</sub> radical.

The Δ<sub>f</sub>H<sub>298</sub> value for methylperoxy seems to be unresolved, relative to CH<sub>3</sub>OOH and the ethyl system. We select a near average value of 2.15 ± 0.91 kcal mol<sup>-1</sup> for CH<sub>3</sub>OO• from experimental data of Knyazev and Slagle<sup>45</sup> and a value of -31.8 ± 0.94 kcal mol<sup>-1</sup><sup>43,46</sup> for CH<sub>3</sub>OOH.

**Reaction Pathways.** A reaction path potential energy diagram is illustrated in Figure 2 calculated at the CBS-Q//B3LYP/6-31G(d,p) level of theory. Addition of oxygen to the ethyl radical forms an energized ethylperoxy adduct.

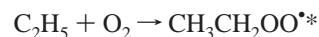


**TABLE 5: Reactions and Rate Constants Used To Build the Current Mechanism To Model Ethyl + O<sub>2</sub> Oxidation<sup>a</sup>**

reaction	A (cm <sup>-3</sup> mol <sup>-1</sup> sec <sup>-1</sup> or sec <sup>-1</sup> )	n	E <sub>a</sub> (cal/mol)	comments	
T5-1	Cl <sub>2</sub> + <i>hν</i> → Cl + Cl				
T5-2	Cl + C <sub>2</sub> H <sub>6</sub> → C <sub>2</sub> H <sub>5</sub> + HCl				
T5-3	CH <sub>3</sub> CH <sub>2</sub> OO* + CH <sub>3</sub> CH <sub>2</sub> OO* → CH <sub>3</sub> CH <sub>2</sub> O* + CH <sub>3</sub> CH <sub>2</sub> O* + O <sub>2</sub>	5.18 × 10 <sup>13</sup>	0.0	225	<i>b, f</i>
T5-4	CH <sub>3</sub> CH <sub>2</sub> OO* + CH <sub>3</sub> CH <sub>2</sub> OO* → CH <sub>3</sub> CHO + CH <sub>3</sub> CH <sub>2</sub> OH + O <sub>2</sub>	3.23 × 10 <sup>10</sup>	0.0	248	<i>d</i>
T5-5	CH <sub>3</sub> CH <sub>2</sub> OO* + HO <sub>2</sub> → CH <sub>3</sub> CH <sub>2</sub> OOH + O <sub>2</sub>	1.64 × 10 <sup>10</sup>	0.0	248	<i>d</i>
T5-6	CH <sub>3</sub> CH <sub>2</sub> OOH → CH <sub>3</sub> CH <sub>2</sub> O* + OH	1.62 × 10 <sup>11</sup>	0.0	-1987	<i>c</i>
T5-7	HO <sub>2</sub> + HO <sub>2</sub> → H <sub>2</sub> O <sub>2</sub> + O <sub>2</sub>	2.5 × 10 <sup>13</sup>	0.0	37700	<i>c</i>
T5-8	C <sub>2</sub> H <sub>6</sub> + OH → C <sub>2</sub> H <sub>5</sub> + H <sub>2</sub> O	1.87 × 10 <sup>12</sup>	0.0	1540	<i>e</i>
T5-9	CH <sub>3</sub> CH <sub>2</sub> O* + O <sub>2</sub> → CH <sub>3</sub> CHO + HO <sub>2</sub>	4.68 × 10 <sup>12</sup>	0.0	2030	<i>c</i>
T5-10	C <sub>2</sub> H <sub>5</sub> + O <sub>2</sub> → CH <sub>3</sub> CH <sub>2</sub> OO*	3.6 × 10 <sup>10</sup>	0.0	1090	<i>c</i>
T5-11	CH <sub>3</sub> CH <sub>2</sub> OO* → C <sub>2</sub> H <sub>5</sub> + O <sub>2</sub>	2.94 × 10 <sup>13</sup>	-0.44	0	<i>g</i>
T5-12	CH <sub>3</sub> CH <sub>2</sub> OO* → *CH <sub>2</sub> CH <sub>2</sub> OOH	2.46 × 10 <sup>18</sup>	-1.07	35320	<i>g</i>
T5-13	*CH <sub>2</sub> CH <sub>2</sub> OOH → CH <sub>3</sub> CH <sub>2</sub> OO*	7.90 × 10 <sup>6</sup>	1.79	35820	<i>g</i>
T5-14	CH <sub>3</sub> CH <sub>2</sub> OO* → CH <sub>3</sub> CHO + OH	1.17 × 10 <sup>7</sup>	1.04	17980	<i>g</i>
T5-15	CH <sub>3</sub> CH <sub>2</sub> OO* → C <sub>2</sub> H <sub>4</sub> + H <sub>2</sub> O	1.32 × 10 <sup>9</sup>	1.37	41590	<i>g</i>
T5-16	CH <sub>3</sub> CH <sub>2</sub> OO* → CH <sub>3</sub> CH <sub>2</sub> O* + O*	8.80 × 10 <sup>5</sup>	2.24	29610	<i>g</i>
T5-17	*CH <sub>2</sub> CH <sub>2</sub> OOH → C <sub>2</sub> H <sub>4</sub> + HO <sub>2</sub>	2.98 × 10 <sup>15</sup>	-0.09	61600	<i>g</i>
T5-18	*CH <sub>2</sub> CH <sub>2</sub> OOH → oxirane + OH	1.28 × 10 <sup>11</sup>	0.52	16150	<i>g</i>
		1.32 × 10 <sup>10</sup>	0.72	15380	<i>g</i>

<sup>a</sup> Reactions T5-1 to T5-9 are reactions from the cited literature sources. Reactions T5-10 to T5-18 are the high-pressure limit rate constants. T5-10 were calculated from variational transition state theory and T5-11 to T5-18 were calculated from canonical transition state theory. <sup>b</sup> Pilgrim, J. S.; McIlroy, A.; Taatjes, C. A. *J. Phys. Chem. A* **1997**, *101*, 1973-1880. <sup>c</sup> Atkinson, R.; Baulch, D. L.; Cox, R. A.; Hampson, R. F., Jr.; Kerr, J. A.; Rossi, M. J.; Troe, J. *J. Phys. Chem. Ref. Data* **1997**, *26*, 521. <sup>d</sup> Wallington, T. J.; Dagaut, P.; Kurylo, M. J. *Chem. Rev.* **1992**, *92*, 667. <sup>e</sup> Baulch, D. L.; Cobos, C. J.; Cox, R. A.; Esser, C.; Frank, P.; Just, Th.; Kerr, J. A.; Pilling, M. J.; Troe, J.; Walker, R. W.; Warnatz, J. *J. Phys. Chem. Ref. Data* **1992**, *21*, 411-429. <sup>f</sup> Clifford, E. P.; Farrel, J. T.; DeSain, J. D.; Taatjes, C. A. *J. Phys. Chem. A* **2000**, *104*, 11549-11560. <sup>g</sup> High-pressure limit rate constant determined in current study.

There are six possible reactions for this activated adduct

- RXN 1) reverse reaction back to reactants
- RXN 2) stabilization
- RXN 3) direct molecular elimination to  
C<sub>2</sub>H<sub>4</sub> + HO<sub>2</sub> (TS1)
- RXN 4) hydrogen shift isomerization to  
hydroperoxy-ethyl adduct (TS2)
- RXN 5) dissociation of O atom to form an  
ethoxy radical plus oxygen atom
- RXN 6) H-shift from ipso carbon to form acetaldehyde  
plus hydroxyl radical (TS5)

RXN 1-3 are important reactions at lower temperature hydrocarbon oxidation. RXN 4 becomes important after HO<sub>2</sub> addition to ethylene (olefins), reverse direction. RXN 3 has an activation barrier of 30.5 kcal mol<sup>-1</sup>, about 4.8 kcal mol<sup>-1</sup> below the ground state starting energy of the reactants. This transition state leads directly to C<sub>2</sub>H<sub>4</sub> + HO<sub>2</sub> products. RXN 4 has a barrier of 36.3 kcal mol<sup>-1</sup>, or about 1 kcal mol<sup>-1</sup> above the reactants C<sub>2</sub>H<sub>5</sub> + O<sub>2</sub>.

The thermodynamic properties for the ethoxy radical in RXN 5 were estimated from group additivity and use of hydrogen bond increment method.<sup>47,48</sup> The products ethoxy + O are estimated to have an endothermicity of over 25 kcal mol<sup>-1</sup> above the reactants and the rate constants at low temperatures would not be significant compared to the other channels, but it is important at high temperatures. The sixth possible channel, RXN 6, for the fate of the activated ethylperoxy adduct is the formation of an aldehyde. The activated ethylperoxy adduct crosses over TS5, which then undergoes OH elimination to form acetaldehyde. The barrier required is 41.7 or 6.4 kcal mol<sup>-1</sup> above the reactants.

The energized hydroperoxyethyl adduct can undergo four different reactions: reverse reaction back to the ethylperoxy radical, stabilization, β-scission to C<sub>2</sub>H<sub>4</sub> + HO<sub>2</sub> products, or

reaction through a three-member ring transition state to form oxirane + hydroxyl. The reverse reaction to the ethylperoxy radical through TS2 has a barrier of about 18.5 kcal mol<sup>-1</sup>. The transition state to form C<sub>2</sub>H<sub>4</sub> + HO<sub>2</sub> (TS3) is about 0.5 kcal mol<sup>-1</sup> higher than that to form oxirane + OH (TS4), based on the CBS-Q//B3LYP/6-31G(d,p) level of theory. Both TS3 and TS4 are below the reactants.

**High-Pressure Limit Arrhenius Rate Parameters (*k*<sub>∞</sub>).** High-pressure limit kinetic parameters in the form of modified Arrhenius rate parameters are included in Table 5 for both forward and reverse reactions. The rate constants are derived from the thermodynamic properties, which consist of enthalpy calculated at the CBS-Q//B3LYP/6-31G(d,p) and entropy and heat capacity values from frequencies and structures at B3LYP/6-31G(d,p) level of theory.

The rate constants for the addition and dissociation reaction for C<sub>2</sub>H<sub>5</sub> + O<sub>2</sub> ⇌ CH<sub>3</sub>CH<sub>2</sub>OO\* are calculated by VTST at B3LYP/6-31G(d,p) level of theory. The reaction coordinate along the C-O bond length is calculated to determine the respective energies. Refer to Figure 1. Rate constants are calculated on the basis of the dissociation path. The addition reaction rate constant is determined by satisfying the detailed balance criteria. The dissociation reaction rate constant is calculated to be *k*<sub>∞,diss</sub> = 2.46 × 10<sup>18</sup>T<sup>-1.07</sup>e<sup>-35.32kcal mol<sup>-1</sup>/RT</sup> and the addition reaction to be *k*<sub>∞,addn</sub> = 2.94 × 10<sup>13</sup>T<sup>-0.44</sup>, with no barrier for the addition path.

**Comparison of Modified Strong Collision Assumption vs Master Equation Results. Major Channels.** Both master equation and modified strong collision treatments of collisional deactivation were employed in our analysis. The predicted effects of pressure (at 297 K) are compared in Figure 3a. Both treatments give nearly identical results. Stabilization is the dominant reaction over the entire range, even at pressures as low as 0.001 atm. The only other channel of importance at this low temperature is the concerted elimination pathway to produce C<sub>2</sub>H<sub>4</sub> + HO<sub>2</sub> (RXN 3). This pathway is predicted to decrease with increased pressure above about 0.01 atm. This decrease in rate coefficient with pressure is due to the increasing importance

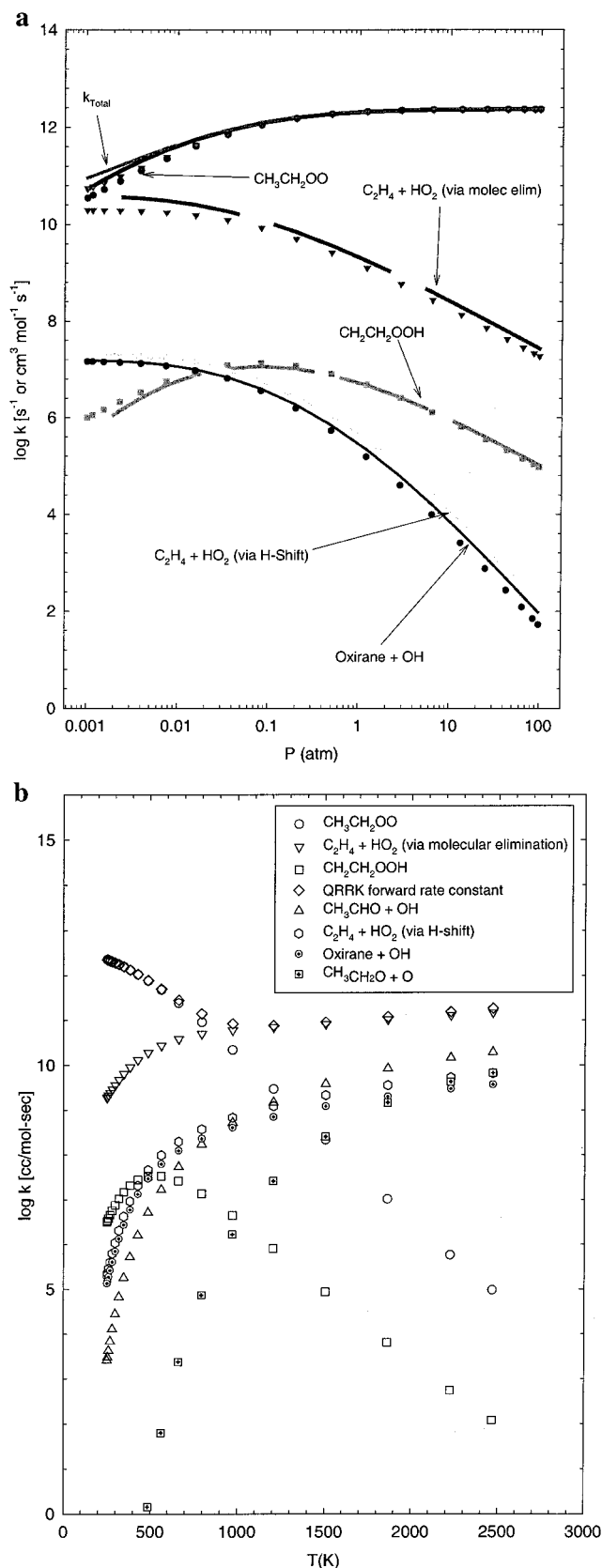


**Figure 3.** Calculated chemical activation rate constants: (a)  $T = 297$  K (symbols = MSC results and lines = ME results); (b)  $P = 0.5$  atm (ME).

of collisional stabilization, which results in deactivation of the energized adduct before the concerted elimination can occur.

**Minor Channels.** For the minor channels, the qualitative behavior is as expected. Stabilization of the hydroperoxyethyl

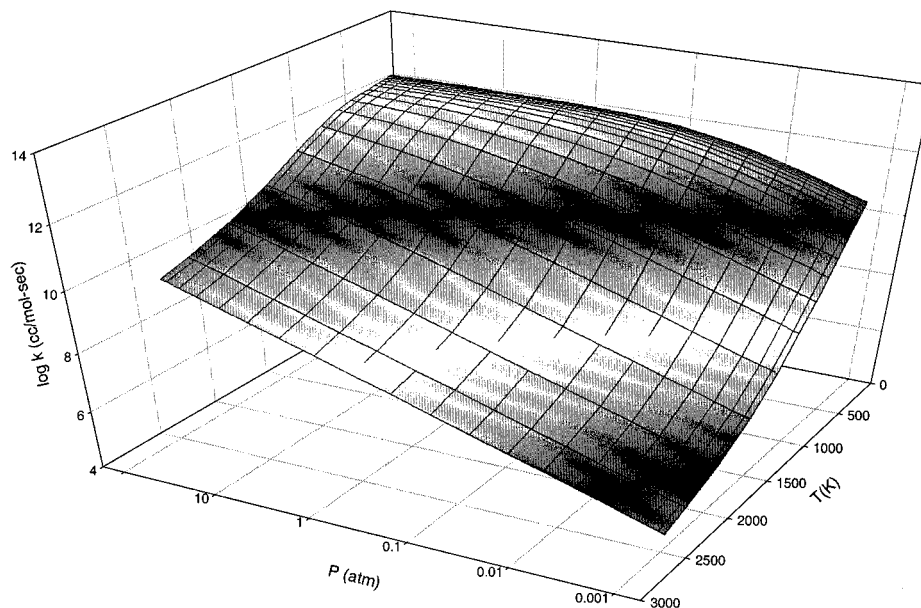
adduct rate goes through a maximum near 0.1 atm. The maximum can be attributed to the fact that the barrier heights of TS3 (formation of  $C_2H_4 + HO_2$ ) and TS4 (formation of oxirane + hydroxyl radical) are lower than that of TS2 (reverse isomerization to ethylperoxy radical). At low pressures, some of the energized  $CH_3CH_2OO^*$  adduct can isomerize to  $^*CH_2CH_2OOH^*$  prior to stabilization, but the subsequent rate of stabilization of  $^*CH_2CH_2OOH^*$  in the low-pressure environment is slower than the rate through TS3 and TS4, so the overall rate for stabilization remains low. As pressure increases, stabilization (primarily  $CH_3CH_2OO^*$ ) becomes more important. But continued increases in pressure diminish the isomerization rate, leading to a decrease in the stabilization rate of  $^*CH_2CH_2OOH$ . The similar rate coefficients for formation of oxirane and ethylene (via the hydrogen shift) reflect similar barriers and A factors for these two channels. This conclusion is similar to that of Green<sup>10</sup> and Shen et al.<sup>15</sup> At this low temperature the reaction to form ethoxy + O is negligible, due to the high endothermicity. We conclude from other modeling studies on the system that a more important path for the  $^*CH_2CH_2OOH$  formation is  $HO_2$  addition to ethylene.<sup>38</sup>

Figure 3b illustrates the results of the master equation predictions for the temperature dependence of the various reaction channels at a fixed pressure of 0.5 atm. The stabilization channel is predicted to dominate at temperatures below approximately 750 K. Above this temperature, the concerted elimination becomes the dominant pathway. As temperature is increased, the rate through other channels begins to increase, while the stabilization rate decreases. Formation of acetaldehyde becomes more rapid at higher temperatures, about 1 order of magnitude slower than the direct molecular elimination channel to form ethylene plus  $HO_2$  at about 2000 K. At the higher temperatures, there is sufficient energy for the energized adduct to overcome the high barrier associated with the four-membered ring TS. The ethoxy radical channel is not important at low temperatures, but rate constant increases rapidly as temperature increases. At 2000 K, the rate constant to form ethoxy radical is less than 2 orders of magnitude slower than the direct molecular elimination channel.

Figure 4 shows the rate coefficient for stabilization of  $CH_3CH_2OO^*$  as a function of both temperature and pressure. A complex temperature–pressure dependence on the stabilization rate constant is apparent. The stabilization rate constant is seen to scale linearly with pressure at temperature greater than 1200 K.

The rate constant for formation of ethylene +  $HO_2$  via molecular elimination is shown in Figure 5. Note the predicted lack of pressure dependence at temperatures above  $\sim 1500$  K. Miller and Klippenstein have also come to a similar conclusion. They predict this rate constant to be independent of pressure above 1000 K.<sup>49</sup> Two channels are competing here: dissociation back to  $C_2H_5 + O_2$  and molecular elimination to  $C_2H_4 + HO_2$ . Collisional stabilization is unimportant even at 100 atm. The predicted rate constants at low temperatures exhibit a negative pressure dependence, consistent with many experimental studies. Kaiser observed a less pronounced pressure dependence on  $C_2H_4$  formation at higher temperatures, with stronger pressure dependence at lower temperatures,<sup>1</sup> similar to the predictions.

**Comparison to Experimental Results.** As indicated earlier, it is necessary to combine the chemical activation with thermal activation reactions that account for the subsequent thermal dissociation of the stabilized adducts. It is also necessary to include reactions of important products that control or limit reverse processes. In Table 5, reactions T5–1 to T5–9 are



**Figure 4.** Surface plot of stabilization rate constant for  $\text{CH}_3\text{CH}_2\text{OO}^*$  as a function of temperature and pressure calculated by QRRK with modified strong collision.

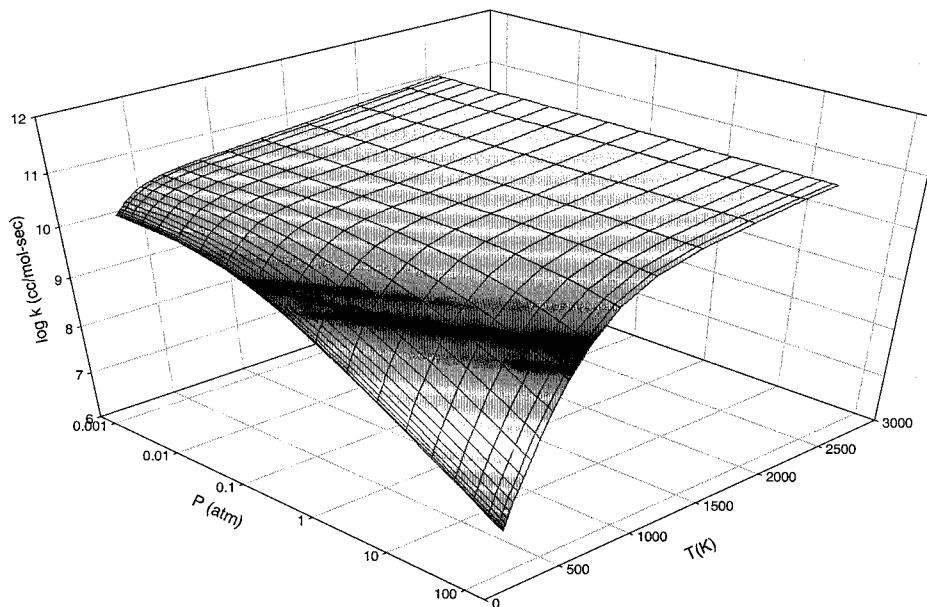


**Figure 5.** Surface plot of direct molecular elimination rate constant for  $\text{C}_2\text{H}_5 + \text{O}_2 \rightarrow \text{C}_2\text{H}_4 + \text{HO}_2$  as a function of temperature and pressure calculated by QRRK with modified strong collision.

included in the mechanism to account for secondary reactions. These same reactions were used in the earlier experimental analysis by Kaiser and by Clifford et al. The pressure-dependent reactions included in the mechanism are listed in Supporting Information Tables 1 and 2. These are calculated in this work. These rate coefficients are listed in the Chebyshev form, with those in Supporting Information Table 1 based on the modified strong collision model for deactivation, and those in Supporting Information Table 2 based on the master equation analysis. In each case, the first seven reactions are for the channels of the energized complex, while the remaining reactions include the thermal dissociation reactions of the two stabilized adducts. For comparison to the data, we used two mechanisms. Both included reactions T5-1 to T5-9, with one using the master equation predictions and the other the modified strong collision predictions. All comparisons with experimental data are done using

the Chebyshev form of the rate constants, unless explicitly stated that the “conventional” form is also used.

**Ethylene Yield.** Comparison of the two different collisional models, i.e., modified strong collision and master equation, with Kaiser’s experimental UV reactor data<sup>1</sup> at 298 K are shown in Figure 6.<sup>1</sup> The two mechanisms are used in the CHEMKIN integrator package to determine the ethylene concentration.<sup>21</sup> Figure 6 shows the comparison of the two predictions to Kaiser’s experimental data for the effect of pressure on the ethylene yield. The error bars on Kaiser’s data are based on secondary consumption corrections that Kaiser estimated to be <12%. Both models show reasonable agreement with Kaiser’s experimental data and properly capture the dramatic drop in yield with increasing pressure. At the higher pressures, the dominant product is formation of the stabilized  $\text{CH}_3\text{CH}_2\text{OO}^*$  adduct (cf. Figure 3a), which does not dissociate at 298 K.

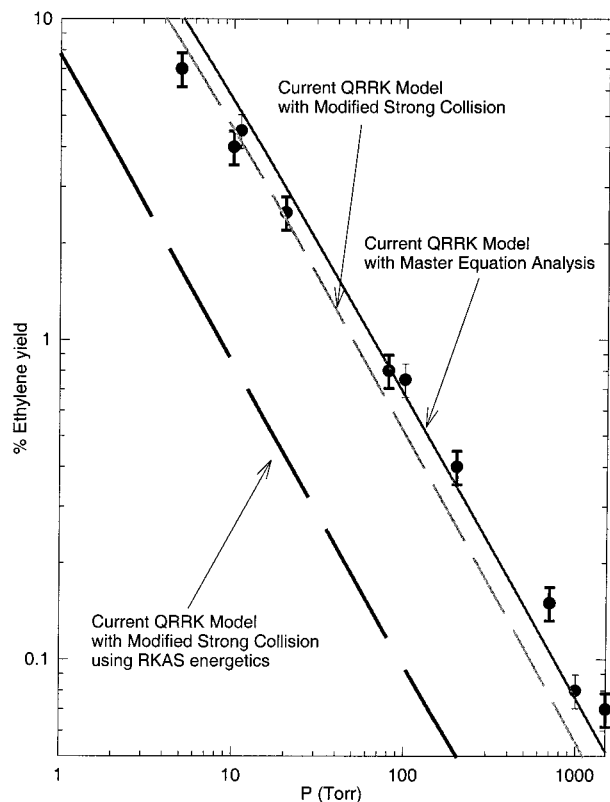


**Figure 6.** Comparison of the pressure effect on  $C_2H_4$  yield at 298 K. Data from Kaiser.<sup>1</sup>

Sensitivity in the ethylene yield to variations in the PE surface (well depth) has been performed, and results are shown in Figure 6. Energetics calculated by RKAS,<sup>17</sup> using the high level coupled cluster ab initio method, are implemented into our QRRK model and the ethylene yield from the calculations using the modified rate constants are compared to Kaiser's experimental data, as shown in Figure 6. RKAS's values for the concerted elimination are  $-0.9 \text{ kcal mol}^{-1}$  (0 K) and  $-2.1 \text{ kcal mol}^{-1}$  (298 K), relative to the entrance channel. Comparison of these results show that the energetics from RKAS underpredict Kaiser's experimental ethylene formation by a factor of 7. Similarly, Miller and Klippenstein also stated that using the energetics from RKAS's calculations in their model also underpredict experimental data by a factor of 7.<sup>49</sup>

The condition shown in Figure 6 is at a low temperature, 298 K. The ethyl +  $O_2$  well depth of over  $32 \text{ kcal mol}^{-1}$  indicates that the only process responsible for the formation of ethylene at 298 K is chemical activation; thermal dissociation from the stabilized adduct will not contribute at this temperature. This allows us to examine the barriers to products, relative to the entrance channel with our model. Our study places the exit channel, via concerted elimination, to be  $-5.7 \text{ kcal mol}^{-1}$  at 298 K below the entrance channel. Miller and Klippenstein, adjusted this barrier in their model to fit the results of Kaiser and determine the best fit to their model to be  $-3.0 \text{ kcal mol}^{-1}$  (at 0 K) below the entrance channel. The  $2.7 \text{ kcal mol}^{-1}$  difference between our current model and that of Miller and Klippenstein is due to the reference temperature. The energetics in our model include the thermal correction from 0 to 298 K. The difference in enthalpy between the concerted elimination transition state and the entrance channel from our calculated CBS-Q//B3LYP/6-31G(d,p) at 0 K is  $-3.7 \text{ kcal mol}^{-1}$ . Our current value, at 0 K, is between the current best fit value of  $-3.0 \text{ kcal mol}^{-1}$  from Miller and Klippenstein<sup>49</sup> and  $-4.3 \text{ kcal mol}^{-1}$  from Miller et al.<sup>18</sup>

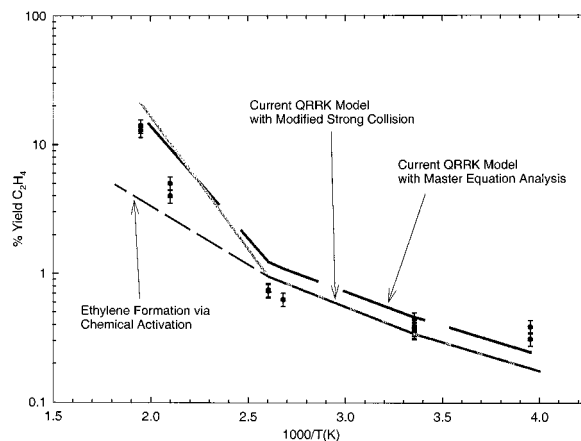


**Figure 7.** Comparison of Kaiser's data at a constant molecular density of  $4.8 \times 10^{18}$  molecule/cc with ME and MSC models.

Comparisons of the predicted and observed temperature dependence of the ethylene yield, at a constant density,  $4.8 \times 10^{18}$  molecules  $\text{cm}^{-3}$ , are shown in Figure 7. Both methods produce reasonable agreement with the experimental data, especially the increase in temperature dependence at higher temperatures. The results for the MSC model are calculated on the basis of the "conventional" CHEMKIN mechanism file format, viz., the non-Chebyshev polynomial formalism. The results for the ME model presented in Figure 7 are calculated on the basis of the Chebyshev polynomial formalism for the CHEMKIN mechanism.

At low temperatures, it is possible to compute the ethylene yield directly by taking the ratio of the sum of the predicted rate coefficients for "direct", i.e., chemically activated, ethylene production to the total predicted "direct" rate coefficient. The temperature is sufficiently low that any contribution from dissociation of the stabilized adduct is insignificant. However, as the temperature is increased and the thermal dissociation rate coefficient increases, it is necessary to include the effects of thermal dissociation of the adduct. The growing importance of the dissociation pathway can be seen in Figure 7 by the difference between the "direct" ethylene yield, based on the MSC model, and the predictions using the mechanism. We see that below 400 K, results from the "direct" and CHEMKIN produce identical results, but at higher temperatures the "direct" ethylene yield is less than the numerical integration results, as the dissociation reactions become important. There are two important dissociation channel of  $CH_3CH_2OO^*$ ,  $C_2H_4 + HO_2$  and  $C_2H_5 + O_2$ ; both need to be considered.

**$HO_2$  Yield.** Experimental data on  $HO_2$  production from Clifford et al.,<sup>2</sup> using laser photolysis, are also compared with the current ME and MSC models. The experiments were carried out from 298 to 700 K at a constant molecular density of  $1.1 \times 10^{18} \text{ cm}^{-3}$ . Clifford et al. present two types of  $HO_2$  concentration yield: total and prompt  $HO_2$  yield. An accurate account of the  $HO_2$  yield has to take into consideration not only the formation of  $HO_2$  but also the amount of  $HO_2$  that is consumed in other reactions, i.e., the  $HO_2$  self-reaction and reaction with the ethylperoxy radical. Figure 8 illustrates an example of the  $HO_2$  concentration profile from CHEMKIN using the MSC mechanism expressed in the "conventional" CHEMKIN mechanism format; CHEMKIN results using the ME mechanism are similar and omitted for clarity.

Predicted  $HO_2$  concentrations, represented by the black circles in Figure 8, show a rapid rise in  $HO_2$  followed by a slower decay before reaching steady state. The shape of this curve is

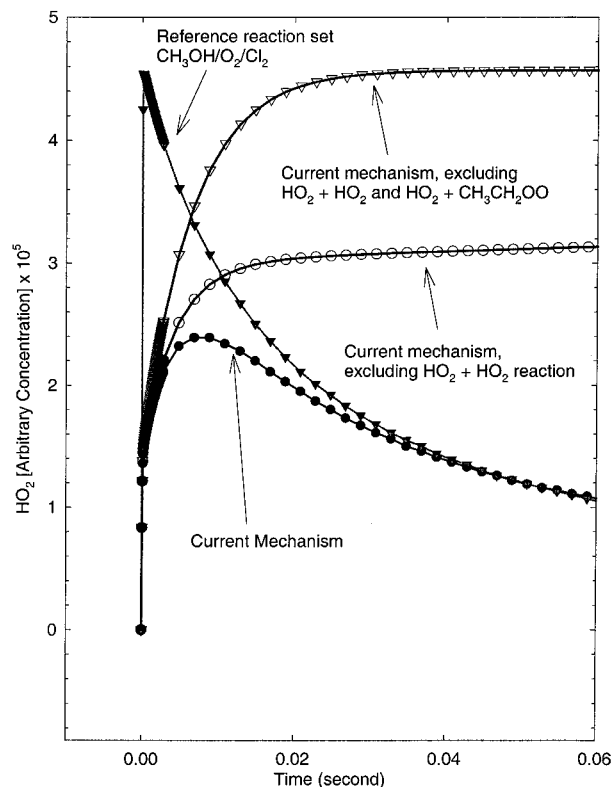


**Figure 8.** Transient HO<sub>2</sub> concentration profile calculated by CHEMKin with our current model.

similar to the actual experimental time-resolved infrared FM signal for HO<sub>2</sub> reported by Clifford et al. Correction of these data for the HO<sub>2</sub> self-reaction (achieved by omitting reaction T5–7), which Clifford et al. term “raw” HO<sub>2</sub>, shows slightly higher initial HO<sub>2</sub> formation followed by a slow increase, also consistent with Clifford et al.’s interpretation. Further correction for the ethylperoxy radical reaction with HO<sub>2</sub> (omitting reaction T5–5) shows an even higher HO<sub>2</sub> formation. This upper curve represents the expected evolution of HO<sub>2</sub> with time, under conditions where there are no HO<sub>2</sub> destruction reactions. Note there is a “prompt” production of HO<sub>2</sub> at very early time, representing formation directly from the initially formed energized ethylperoxy radical. This is followed by a much slower rise, and this can be attributed to the slower production of HO<sub>2</sub> from the *stabilized* ethylperoxy radical. Clifford et al. accounted for the secondary reactions of HO<sub>2</sub> by comparing their observed HO<sub>2</sub> production to that obtained using •CH<sub>2</sub>OH from methanol as a reactant, since the HO<sub>2</sub> yield from •CH<sub>2</sub>OH is expected to be unity. In our calculations, we obtained our HO<sub>2</sub> yields in a similar manner.

A comparison of the “prompt” HO<sub>2</sub> yield between Clifford et al.’s experimental data, at a constant total molecular density of  $1.1 \times 10^{18}$  molecule cm<sup>-3</sup>, and the numerical integration results from the ME and MSC mechanisms is shown in Figure 9. The results using both master equation and modified strong collision treatments are similar and slightly lower than observed.

Figure 10 compares the predicted “total” HO<sub>2</sub> yield as a function of temperature to that measured by Clifford et al. The results from both the ME and MSC are similar and agree very well with the observations of Clifford et al. Particularly encouraging is the correct prediction of the observed rapid increase near 600 K. At the higher temperatures, only a small fraction of the total HO<sub>2</sub> is predicted to come directly from the energized adduct; the dominant pathway is dissociation of the

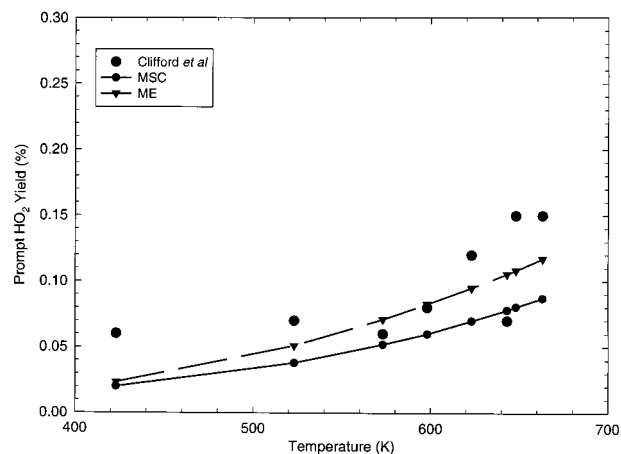


**Figure 9.** Comparison of formation of “prompt” HO<sub>2</sub> between Clifford et al.’s experimental data and predictions using the mechanisms. Clifford et al.’s data are shown as filled circles, ME mechanism is given as the dashed line (with inverted triangles), and MSC mechanism is the solid line (with circles).

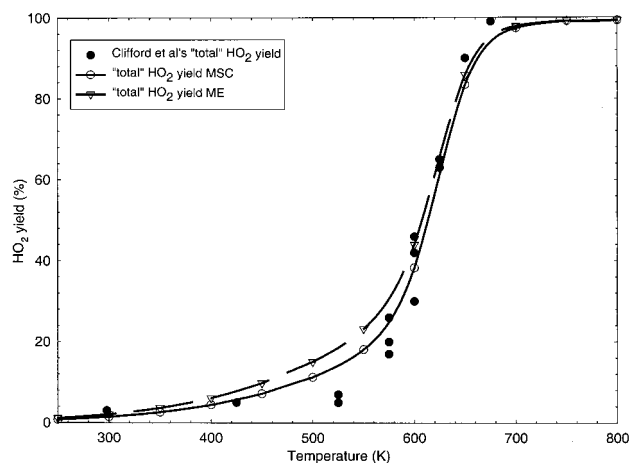
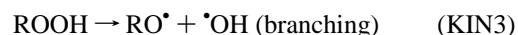


**Figure 10.** Comparison of master equation and modified strong collision model predictions with data for “total” HO<sub>2</sub> formation: (filled circle) Clifford et al.’s data; (dashed line with inverted triangles) ME; (solid line with circles) MSC.

initially stabilized adduct. Failure to account for this dissociation in the mechanism would lead to a substantial error.

#### Kinetic Implications for Low Temperature Ignition

The conventional approach to describe low-temperature ignition kinetics, especially the region of negative temperature coefficient, considers the following reactions:<sup>50</sup>



(R<sup>•</sup> is an alkyl radical, RO<sup>•</sup> is an alkoxy radical, and yRO is generally a cyclic ether. R<sup>•</sup>OOH is often written as QOOH, but we use the R<sup>•</sup>COOH notation to emphasize the free radical

character of this species.) If the temperature is sufficiently low that the equilibrium in KIN1 is shifted to the right, the subsequent reactions of RO<sub>2</sub> can lead to the chain-branching (KIN3 and KIN6) needed for ignition. However, as the temperature rises, the equilibrium in KIN1 shifts to the left, reducing the RO<sub>2</sub> concentration and thus slowing down the overall rate, i.e., producing a negative temperature coefficient of reaction rate. Particularly noteworthy in this mechanism is the importance of the isomerization reaction (KIN4); without this, chain branching via KIN6 cannot occur. In ethane oxidation, the *newly identified* direct pathway for production of ethylene and HO<sub>2</sub> from ethylperoxy is much faster than KIN4. This competing fast reaction necessarily reduces the amount of R'COOH that can be produced via KIN4. (One specific illustration is shown in Figure 3b, where •CH<sub>2</sub>CH<sub>2</sub>OOH is approximately 3 orders of magnitude lower than CH<sub>3</sub>CH<sub>2</sub>OO•.) Thus the amount of chain branching via KIN6 will be substantially reduced. Although more complex fuels might well have lower barriers to isomerization [by having the internal hydrogen transfer proceed through a less strained ring (six- or seven- vs five-member) or by abstracting secondary or tertiary hydrogens rather than the primary hydrogens in ethyl], the possibility of concerted elimination of HO<sub>2</sub> from RO<sub>2</sub> in these fuels will generally result in formation of less R'COOH and this will reduce the overall branching rates. Thus there is a need to revisit these systems to see if new branching pathways are needed to accurately describe low-temperature ignition.

## Conclusions

Thermodynamic properties for the reaction system of ethyl radical plus molecular oxygen have been calculated by the ab initio composite method, G2 and CBS-Q//B3LYP/6-31G(d,p). The enthalpies calculated by CBS-Q//B3LYP/6-31G(d,p) shows that the molecular elimination transition state is lower than the reactants by 4.8 kcal mol<sup>-1</sup> and that the hydrogen shift transition state is higher than the reactants by about 1 kcal mol<sup>-1</sup>. The association and dissociation reaction rate constants are determined by VTST and detailed balance criteria. The other high-pressure rate constants are determined from canonical transition state theory. This reaction system was analyzed in terms of both the initial product distribution resulting from the reactions of the *energized* CH<sub>3</sub>CH<sub>2</sub>OO• adduct and the subsequent thermal dissociation of the *stabilized* CH<sub>3</sub>CH<sub>2</sub>OO• adduct. This analysis was performed by using a QRRK formalism for *k*(*E*) coupled with either a modified strong collision model (MSC) or a master equation model (ME) to account for collisional deactivation. These models used unadjusted input parameters based exclusively on electronic structure calculations with adduct enthalpies from isodesmic working reactions. Comparison of predictions from these models to experimental observations for both ethylene and HO<sub>2</sub> yields were generally very satisfactory, with little differences in the MSC and ME predictions.

The utility of a Chebyshev formalism to represent both the temperature and pressure dependence of the rate coefficients for use within a CHEMKIN mechanism was demonstrated. The Chebyshev polynomial mechanism is a promising method to model complex pressure dependent systems.

## Appendix: Solution of Master Equation

A formalism is desired which conceptually “hides” the *E* dependence of the master equation. First, (MEM3) is

rearranged to

$$f_i^q = (k_i^q + \omega)n_i^q - \omega \sum_r P_i^{qr} n_r^q - \sum_j k_{ij}^q n_j^q \quad (\text{A1})$$

where the notation has been simplified by the definition of a total differential rate constant out of level (*i*, *q*) due to reaction,

$$k_i^q = \sum_p d_{p,i}^q + \sum_j k_{ji}^q \quad (\text{A2})$$

A matrix notation is now introduced in which a single bar represents an *E* vector and a double bar indicates an *E* matrix. Equation A1 can then be written

$$\begin{bmatrix} \bar{f}_1 \\ \bar{f}_2 \\ \vdots \\ \bar{f}_n \end{bmatrix} = \begin{bmatrix} \bar{J}_{11} & -\bar{k}_{12} & \cdots & -\bar{k}_{1n} \\ -\bar{k}_{21} & \bar{J}_{22} & \cdots & -\bar{k}_{2n} \\ \vdots & \vdots & \ddots & \vdots \\ -\bar{k}_{n1} & -\bar{k}_{n2} & \cdots & \bar{J}_{nn} \end{bmatrix} \begin{bmatrix} \bar{n}_1 \\ \bar{n}_2 \\ \vdots \\ \bar{n}_n \end{bmatrix} \quad (\text{A3})$$

The matrix components of (A3) can be related to the earlier notation, via

$$\begin{aligned} (\bar{J}_{ii})_{qr} &= (k_i^q + \omega)\delta_{qr} - \omega P_i^{qr} \\ (\bar{k}_{ij})_{qr} &= k_{ij}^q \delta_{qr} \\ (\bar{f}_i)_q &= f_i^q, (\bar{n}_i)_q = n_i^q \end{aligned} \quad (\text{A4})$$

Note that in (A3), the differential isomerization rate constants are expressed as (diagonal) matrices in *E* space; the reason for this will become apparent later.

Equation (A3) now looks like a standard matrix equation. The solution necessitates the inversion of this equation. This can be written symbolically as

$$\mathbf{n} = (\mathbf{J})^{-1} \mathbf{f} \quad (\text{A5})$$

where a second notation has been introduced in which bold variables are vectors and matrices in isomer space. Due to the complexities of the components, the matrix inversion implied by (A5) is not quite defined. However, Carter and Tardy<sup>36</sup> show explicit expressions can be written if this is treated as a 2 × 2 matrix equation. This is done by writing this equation in terms of submatrices,

$$\begin{bmatrix} \bar{f}_1 \\ \mathbf{f}_2 \end{bmatrix} = \begin{bmatrix} \bar{J}_{11} & -\mathbf{k}_{12} \\ -\mathbf{k}_{21} & \mathbf{J}_{22} \end{bmatrix} \begin{bmatrix} \bar{n}_1 \\ \mathbf{n}_2 \end{bmatrix} \quad (\text{A6})$$

where

$$\begin{aligned} \mathbf{f}_2 &= \begin{bmatrix} \bar{f}_2 \\ \bar{f}_3 \\ \vdots \\ \bar{f}_n \end{bmatrix} & \mathbf{n}_2 &= \begin{bmatrix} \bar{n}_2 \\ \bar{n}_3 \\ \vdots \\ \bar{n}_n \end{bmatrix} & \mathbf{k}_{21} &= \begin{bmatrix} \bar{k}_{21} \\ \bar{k}_{31} \\ \vdots \\ \bar{k}_{n1} \end{bmatrix} \\ \mathbf{k}_{12} &= [\bar{k}_{12} \quad \bar{k}_{13} \quad \cdots \quad \bar{k}_{1n}] & \mathbf{J}_{22} &= \begin{bmatrix} \bar{J}_{22} & -\bar{k}_{23} & \cdots & -\bar{k}_{2n} \\ -\bar{k}_{32} & \bar{J}_{33} & \cdots & -\bar{k}_{3n} \\ \vdots & \vdots & \ddots & \vdots \\ -\bar{k}_{n2} & -\bar{k}_{n3} & \cdots & \bar{J}_{nn} \end{bmatrix} \end{aligned} \quad (\text{A7})$$

Carter and Tardy derive expressions for two components of **n** ( $\bar{n}_1, \mathbf{n}_2$ ), which involve inverses of the submatrices  $\bar{J}_{11}$  and  $\mathbf{J}_{22}$ .  $\bar{J}_{11}$  is strictly a matrix in *q* space, so its inverse can be computed by standard numerical techniques.  $\mathbf{J}_{22}$  is just as complicated as



the original  $\mathbf{J}$ ; yet the identical procedure can be employed to compute its inversion as that of  $\mathbf{J}$  itself. Carter and Tardy implement their procedure through a FORTRAN code that actually writes explicit, problem-dependent algorithms in the form of a second FORTRAN code. Here we merely note the theory can be implemented just as written, i.e., recursively. This simplified prescription is thus presented here, with minimum commentary (again see Carter and Tardy for the derivation).

In what follows, the  $\leftarrow$  operator is used in place of the  $=$  sign to signify assignment, as used in programming. The first step is compute

$$\bar{n}_1 \leftarrow (1/\bar{J}_{11})\bar{f}_1 \quad (\text{A8})$$

Here, the  $1/\bar{J}$  notation is used to denote a matrix inverse in  $q$  space. Equation A8 can be evaluated through standard linear algebra techniques. Second, the compound expression is evaluated,

$$\mathbf{n}_2 \leftarrow \mathbf{k}_{21}\bar{n}_1 + \mathbf{f}_2 \quad (\text{A9})$$

In the current matrix notation this signifies the set of equations ( $\bar{n}_i \leftarrow \bar{k}_{i1}\bar{n}_1 + \bar{n}_i, i = 2, n$ ). Next the submatrix  $\mathbf{J}_{22}$  is modified,

$$\mathbf{J}_{22} \leftarrow \mathbf{J}_{22} - \mathbf{k}_{21}(1/\bar{J}_{11})\mathbf{k}_{12}. \quad (\text{A10})$$

Note this signifies that an operation that is performed on every component of  $\bar{\mathbf{J}}_{22}$ , both diagonal and off diagonal ( $\bar{J}_{22} \leftarrow \bar{J}_{22} - \bar{k}_{21}(1/\bar{J}_{11})\bar{k}_{12}$ ;  $\bar{k}_{23} \leftarrow \bar{k}_{23} - \bar{k}_{21}(1/\bar{J}_{11})\bar{k}_{13}$ , etc.). This is why allowance must be made so that the  $\bar{k}$  matrices are two-dimensional in  $E$ .

The next step is to perform the matrix inversion on the modified  $\mathbf{J}_{22}$ ,

$$\mathbf{n}_2 \leftarrow (\mathbf{J}_{22})^{-1}\mathbf{n}_2 \quad (\text{A11})$$

The new value of  $\mathbf{n}_2$  is used to compute the final value of  $\bar{n}_1$  through

$$\bar{n}_1 \leftarrow \bar{n}_1 + (1/\bar{J}_{11})\mathbf{k}_{12}\mathbf{n}_2 \quad (\text{A12})$$

Note eq A11 is quite similar to (A6), except the (current) value of  $\mathbf{n}_2$  is in place of the original input vector  $\mathbf{f}_2$ , and there is one less dimension to the problem. The procedure outlined by eqs A8 through A12 can thus be used to solve (A11). In this second iteration, eq A11 would be invoked to invert  $\mathbf{J}_{33}$ , and so forth. The recursion effectively peels off one layer at a time until the innermost layer is reached. The final inversion,

$$\bar{n}_n \leftarrow (1/\bar{J}_{nn})\bar{n}_n, \quad (\text{A13})$$

can be done explicitly.

Fortunately, throughout these convoluted manipulations, vectors and matrices never need to have their old values saved. This averts placing additional burdens on computer memory requirements. One minor nuisance is that some computer languages, such as FORTRAN, do not allow explicit recursion. Luckily, the total number of recursive calls is not large (equal to one less the number of possible isomers) so recursion can be readily implemented using duplicate subroutines.

**Supporting Information Available:** Tables of pressure dependent rate constants, total energies, zero-point vibrational energies, and thermal corrections, and rotational barriers and

moments of inertia. This material is available free of charge via the Internet at <http://pubs.acs.org>.

## References and Notes

- (1) Kaiser, E. W. *J. Phys. Chem.* **1995**, *99*, 707.
- (2) Clifford, E. P.; Farrell, J. T.; DeSain, J. D.; Taatjes, C. A. *J. Phys. Chem. A* **2000**, *104*, 11549.
- (3) Slagle, I. R.; Feng, Q.; Gutman, D. *J. Phys. Chem.* **1984**, *88*, 3648.
- (4) Slagle, I. R.; Ratajczak, E.; Gutman, D. *J. Phys. Chem.* **1986**, *90*, 402.
- (5) McAdam, G. K.; Walker, R. W. *J. Chem. Soc., Faraday Trans. 2* **1987**, *83*, 1509.
- (6) Plumb, I. C.; Ryan, K. R. *Int. J. Chem. Kinet.* **1981**, *13*, 1011.
- (7) Gutman, D. *J. Chem. Phys.* **1987**, *84*, 409.
- (8) Kaiser, E. W.; Rimai, L.; Wallington, T. J. *J. Phys. Chem.* **1989**, *93*, 4094.
- (9) Bozzelli, J. W.; Dean, A. M. *J. Phys. Chem.* **1990**, *94*, 3313.
- (10) Green, W. H. *Int. J. Quantum Chem.* **1994**, *52*, 837.
- (11) Ignatyev, I. S.; Xie, Y.; Allen, W. D.; Schaefer, H. F. *J. Chem. Phys.* **1997**, *107*, 141.
- (12) Quelch, G. E.; Gallo, M. M.; Schaefer, H. F., III. *J. Am. Chem. Soc.* **1992**, *114*, 8239.
- (13) Wagner, A. F.; Slagle, I. R.; Sarzynski, D.; Gutman, D. *J. Phys. Chem.* **1990**, *94*, 1853.
- (14) Atkinson, D. B.; Hudgens, J. W. *J. Phys. Chem. A* **1997**, *101*, 3901.
- (15) Shen, D.; Moise, A.; Pritchard, H. O. *J. Chem. Soc., Faraday Trans.* **1995**, *91*, 1425.
- (16) Skancke, A.; Skancke, P. N. *J. Mol. Struct. (THEOCHEM)* **1990**, *207*, 201.
- (17) Rienstra-Kiracofe, J. C.; Allen, W. D.; Schaefer, H. F., III. *J. Phys. Chem. A* **2000**, *104*, 9823.
- (18) Miller, J. A.; Klippenstein, S. J.; Robertson, S. H. A Theoretical Analysis of the Reaction Between Ethyl and Molecular Oxygen. 28th International Symposium on Combustion, 2000, Edinburgh, Scotland.
- (19) Venkatesh, P. K.; Dean, A. M.; Cohen, M. H.; Carr, R. W. *Rev. Chem. Eng.* **1997**, *13*, 1.
- (20) Venkatesh, P. K.; Chang, A. Y.; Dean, A. M.; Cohen, M. H.; Carr, R. W. *AIChE J.* **1997**, *43*, 1331.
- (21) Kee, R. J.; Rupley, F. M.; Miller, J. A. Chemkin-II: A Fortran Chemical Kinetics Package for the Analysis of Gas-Phase Chemical Kinetics. Sandia National Laboratories, 1989.
- (22) Ochterski, J. W.; Petersson, G. A.; Montgomery, J. A. *J. Chem. Phys.* **1996**, *104*, 2598.
- (23) Frisch, M. J.; Trucks, G. W.; Head-Gordon, M.; Gill, P. M. W.; Wong, M. W.; Foresman, J. B.; Johnson, B. G.; Schlegel, H. B.; Robb, M. A.; Replogle, E. S.; Gomperts, R.; Andres, J. L.; Raghavachari, K.; Binkley, J. S.; Gonzalez, C.; Martin, R. L.; Fox, D. J.; Defrees, D. J.; Baker, J.; Stewart, J. J. P.; Pople, J. A. *Gaussian 94*, Revision C.2; Gaussian Inc.: Pittsburgh, PA, 1995.
- (24) Becke, A. D. *J. Chem. Phys.* **1993**, *98*, 5648.
- (25) Lee, C.; Yang, W.; Parr, R. G. *Phys. Rev. B* **1988**, *37*, 785.
- (26) Scott, A. P.; Radom, L. *J. Phys. Chem.* **1996**, *100*, 16502.
- (27) Hehre, W. J.; Radom, L.; Schleyer, P. R.; Pople, J. A. *Ab Initio Molecular Orbital Theory*; Wiley & Sons: New York, 1986.
- (28) Curtiss, L. A.; Raghavachari, K.; Trucks, G. W.; Pople, J. A. *J. Chem. Phys.* **1991**, *94*, 7221.
- (29) Pitzer, K. S.; Gwinn, W. D. *J. Chem. Phys.* **1942**, *10*, 428.
- (30) Gilbert, R. G.; Luther, K.; Troe, J. *Ber. Bunsen-Ges. Phys. Chem.* **1983**, *87*, 169–177.
- (31) Chang, A. Y.; Bozzelli, J. W.; Dean, A. M. *Z. Phys. Chem.* **2000**, *1533*.
- (32) Ritter, E. R. *Int. J. Chem. Kinet.* **1997**, *29*, 161.
- (33) Ritter, E. R. *J. Chem. Inf. Comput. Sci.* **1991**, *31*, 400.
- (34) Bozzelli, J. W.; Dean, A. M.; Chang, A. *Int. J. Chem. Kinet.* **1997**, *29*, 161.
- (35) Reid, R. C.; Prausnitz, J. M.; Poling, B. E. *The Properties of Gases and Liquids*, 4th ed.; McGraw-Hill: New York, 1987.
- (36) Carter, W. P.; Tardy, D. C. *J. Phys. Chem.* **1974**, *78*, 1579.
- (37) Gilbert, R. G.; Smith, S. C. *Theory of Unimolecular and Recombination Reactions*; Blackwell Scientific Publications: Oxford, U.K., 1990.
- (38) Chen, C.-J.; Bozzelli, J. W. *J. Phys. Chem. A* **2000**, *104*, 4997.
- (39) Dobis, O.; Benson, S. W. *J. Phys. Chem. A* **1997**, *101*, 6030.
- (40) Marshall, P. J. *J. Phys. Chem. A* **1999**, *103*, 4560.
- (41) Quelch, G. E.; Gallo, M. M.; Shen, M.; Xie, Y.; Schaefer, H. F.; Moncrieff, D. *J. Am. Chem. Soc.* **1994**, *116*, 4953.
- (42) Blanksby, S. J.; Ramond, T. M.; Davico, G. E.; Nimlos, M. R.; Kato, S.; Bierbaum, V. M.; Lineberger, W. C.; Ellison, G. B.; Okumura, M. *J. Am. Chem. Soc.* **2001**, *123*, 9585.
- (43) Sun, H.; Chen, C.-J.; Bozzelli, J. W. *J. Phys. Chem. A* **2000**, *104*, 8270.

- (44) Brinks, T.; Lee, H.-N.; Jonsson, M. *J. Phys. Chem. A* **1999**, *103*, 7094.
- (45) Knyazev, V. D.; Slagle, I. R. *J. Phys. Chem. A* **1998**, *102*, 1770.
- (46) Lay, T. H.; Bozzelli, J. W. *J. Phys. Chem. A* **1997**, *101*, 9505.
- (47) Lay, T. H.; Bozzelli, J. W.; Dean, A. M.; Ritter, E. R. *J. Phys. Chem.* **1995**, *99*, 14514.

- (48) Benson, S. W. *Thermochemical Kinetics*, 2nd ed.; Wiley-Interscience: New York, 1976.
- (49) Miller, J. A.; Klippenstein, S. J. *Int. J. Chem. Kinet.* **2001**, *33*, 654.
- (50) Walker, R. W.; Morley, C. Basic Chemistry of Combustion. In *Low-Temperature Combustion and Autoignition*; Pilling, M. J., Ed.; Elsevier: Amsterdam; New York, 1997; p 1.